

## ABSTRACT

Title of thesis: A DEMONSTRATION OF GLASS BONDING  
USING PATTERNED NANOCOMPOSITE  
THERMITES DEPOSITED FROM FLUID

Juan Carlos Rodriguez, Master's of Science, 2015

Thesis directed by: Professor Michael Zachariah  
Department of Chemistry and Biochemistry

Ceramics and other nonmetals are widely used in industrial and research applications. Although these materials provide many advantages, they often pose unique challenges during bonding. This work aims to expand on current processes, which have much narrower applications, to find a more universal method for nonmetal bonding. We utilize inks comprised of aluminum-based nanoenergetics (a heat source) and tin (a bonding agent). Requirements for successful bonding are explored and four key criteria are established. Through statistical simulation and thermochemical equilibrium calculations, we conclude that the presence of a diluent in large percentages negatively impacts reaction kinetics. Conversely, we show small percentages of added tin enhance gas generation and drive faster reaction rates. The bulk bonding material, thermite plus tin, forms a continuous structure during reaction, adhering well to the substrate surface. In some cases, these bonds failed above 1200 kPa.

A DEMONSTRATION OF GLASS BONDING USING  
PATTERNED NANOCOMPOSITE THERMITES DEPOSITED  
FROM FLUID

by

Juan Carlos Rodriguez

Thesis submitted to the Faculty of the Graduate School of the  
University of Maryland, College Park in partial fulfillment  
of the requirements for the degree of  
Master's of Science  
2015

Advisory Committee:  
Professor Michael Zachariah, Chair/Advisor  
Professor Bao Yang  
Professor Christopher Cadou

© Copyright by  
Juan Rodriguez  
2015

## Acknowledgments

I would like to thank Dr. Zachariah for all his of guidance and suggesting this stimulating research topic, as well as Alex Tappan for his input throughout this process. I am also appreciative of the support of my family and co-workers who made this experience enjoyable. I would like to express my deep gratitude to Sandia National Laboratories and the National Physical Science Consortitium for their financial support. I would also like to acknowledge the support of the Maryland NanoCenter.

## Contents

1. <i>Introduction</i> . . . . .	1
1.1 Introduction To Thermites . . . . .	1
1.2 A Brief History of Welding and Joining With Thermites . . . . .	5
1.2.1 Joining Ceramics and Non-Metals . . . . .	5
1.2.2 Welding and Joining With Nanomaterials . . . . .	9
1.3 Bonding Criteria . . . . .	10
2. <i>Methods</i> . . . . .	14
2.1 Pressure Cell Measurements and Thermochemical Modeling . . . . .	15
2.2 Deposition . . . . .	17
2.2.1 Electrospray . . . . .	17
2.2.2 Direct Write . . . . .	20
2.3 Combustion Velocity . . . . .	24
2.4 Bond Strength . . . . .	26
3. <i>Results</i> . . . . .	28
3.1 Pressure Cell Measurements and Thermochemical Modeling . . . . .	28
3.2 Combustion Velocity Results . . . . .	34
3.3 Bonding . . . . .	37
3.4 Stress Testing . . . . .	45
4. <i>Conclusion</i> . . . . .	51

## List of Tables

1.1	Overview of common thermite reactions, reproduced from [14]	2
2.1	Summary of reactant properties	15

## List of Figures

1.1	Maximum enthalpies of combustion of selected energetic materials, reproduced from [11] . . . . .	3
1.2	Diagram of proposed bonding system requirements . . . . .	12
2.1	Diagram of constant volume experiment, reproduced from [40] . . . . .	16
2.2	Number of layers vs. total weight, thickness, and width . . . . .	23
2.3	Profile of ideal line . . . . .	23
2.4	Profile of rounded line . . . . .	23
2.5	Profile of line with channel and material pushed to side . . . . .	24
2.6	Profile of line with channel and flat top . . . . .	24
2.7	Burn speed experimental setup as viewed by the camera . . . . .	25
2.8	Diagram of stress test . . . . .	26
3.1	Pressure and optical signals for combustion of pure Al/WO <sub>3</sub> . . . . .	29
3.2	Pressure and optical signals for combustion of Al/WO <sub>3</sub> + 100% tin . . . . .	29
3.3	Peak pressure magnitude (experimental and calculated) and adiabatic temperature (calculated) as a function of added tin . . . . .	30
3.4	Relationship between peak pressure time and peak optical time . . . . .	32
3.5	Burning time as a function of added tin. . . . .	33
3.6	Combustion velocity as a function of thickness for 0%, 50%, and 100% added tin . . . . .	35
3.7	Interface diagram for an ideal six particle system . . . . .	36
3.8	Interfaces, as a percentage of ideal, vs. added tin . . . . .	37
3.9	Average length of tin string as a function of added tin . . . . .	37
3.10	Figures of substrates post reaction . . . . .	38
3.11	Large hole in bonding material structure caused by excessive gas generation . . . . .	39
3.12	Thermal profile into substrate . . . . .	41
3.13	Heat of reaction vs. added tin . . . . .	42
3.14	Continuous bonding material layer is porous on a micron-scale . . . . .	43
3.15	Tungsten silicon system phase diagram . . . . .	44
3.16	EDS line scan of substrate surface bonding . . . . .	45
3.17	EDS map showing tungsten silicon alloying away from substrate surface . . . . .	45
3.18	Shear strength vs. thickness for 50% and 100% added nanotin . . . . .	47
3.19	The bonding material remains attached to both sides of the substrate during the first type of failure mechanism. . . . .	48

3.20 Thermal fractures seen in substrates (1) . . . . .	49
3.21 Thermal fractures seen in substrates (2). . . . .	50
3.22 Fragments of adjacent substrate remains bonded to bulk bonded region.	50



## Chapter 1: Introduction

### *1.1 Introduction To Thermites*

The thermite reaction was first described by German Hans Goldschmidt in 1897 and later patented as a means of producing metals and alloys. Goldschmidt noted the reaction was “...very energetic...” to the point that material was “...thrown out of the crucible...” [17]. A thermite reaction takes place between a metal (the fuel) and a metal oxide (the oxidizer). The reaction forms a more stable oxide and releases a significant amount of heat. This general reaction is depicted in Equation 1.1. In this equation M is the fuel (metal or alloy), with corresponding oxide MO, and A is the oxidizer (metal or alloy), with corresponding oxide AO. The heat released is denoted by  $\Delta H$  [44].



The amount of heat released and the adiabatic reaction temperature are largely dependent on the fuel and oxidizer combination and are summarized in Table 1.1 (reproduced from [14]) for several common combinations. These high-energy reactions are used in a variety of military and civilian applications including bulk metal welding [18], cutting torches [16], hand held incendiary devices [38], and large scale

incendiary bombs [20].

*Tab. 1.1: Overview of common thermite reactions, reproduced from [14].*

Constituents	Adiabatic Reaction Temperature	Heat of Reaction	
	T (K)	$-Q \left( \frac{\text{cal}}{\text{g}} \right)$	$-Q \left( \frac{\text{cal}}{\text{cm}^3} \right)$
2Al + 3CuO	2843	974.1	4976
2Al + Fe <sub>2</sub> O <sub>3</sub>	3135	945.4	3947
2Al + Bi <sub>2</sub> O <sub>3</sub>	3253	506.1	3638
2Al + WO <sub>3</sub>	3253	696.4	3801
4Al + 3(O <sub>2</sub> ) <sub>g</sub>	4019	7857	1.424

Reactant particle size has a large effect on the reaction rate and reaction mechanisms. Goldschmidt was the first to note this principle in his original patent. He stated “the aluminum should be employed in a finely-pulverized state if the result is to be a success” [17]. Further research in this area demonstrated that the reaction rate between the metal and the oxide is largely dependent on the mass diffusion rate and therefore the particle size of the reactant species. Traditional thermite reactions take place between micron-scale fuel and oxidizer particles. Research shows that these large particles result in a slow reaction rate [35, 43]. In addition, micron-scale particles are insensitive to ignition and have a significant ignition delay.

More recently, effort has been put into decreasing particle size. These efforts strive

to bring the reaction rates and ignition characteristics between metal and oxide particles closer to those of monomolecular high-energy materials. Monomolecular energetic materials contain fuel and oxidizer species within the same molecule, separated by angstrom-scale chemical bonds. These short diffusion distances allow for very fast reaction rates and relatively little ignition delay. However, these monomolecular energetic materials have relatively low energy density, both in terms of mass and volume, compared to metal fuels. This is shown in Figure 1.1 (reproduced from [11]).

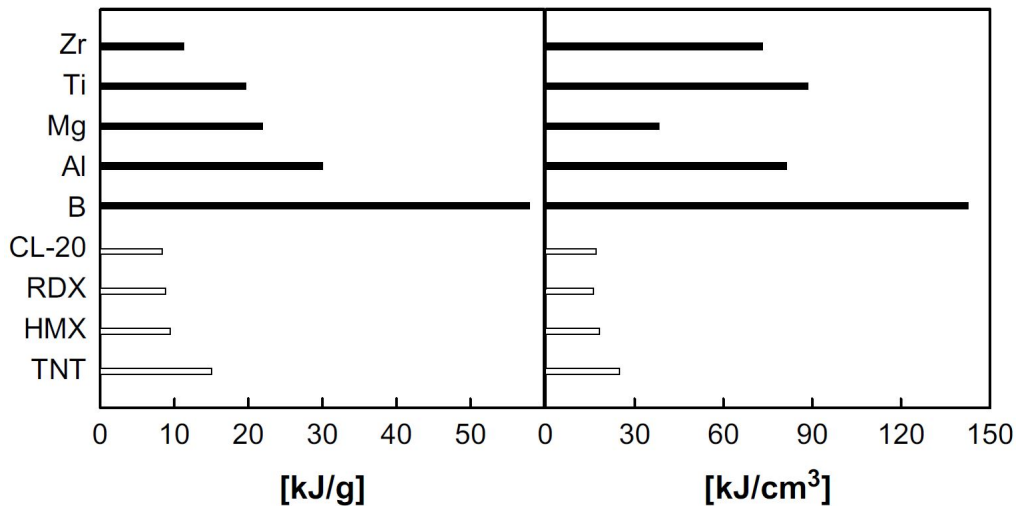


Fig. 1.1: Maximum enthalpies of combustion of selected energetic materials, reproduced from [11]. Reprinted from Progress in Energy and Combustion Science, Volume 35 / Issue 2, Edward L. Dreizin, Metal-based reactive nano-materials, Page 142., Copyright (2008), with permission from Elsevier.

In an ideal scenario, the short diffusion distances of monomolecular materials would be combined with the high energy density of metals. Nanothermites were developed to meet this aim [7]. Nanothermites consist of nanoscale metal fuel and metal oxide particles that have the same general reaction shown in Equation 1.1. Although

nanothermites are not a perfect blend of the desired energetic properties, as they are not as intimately mixed as monomolecular materials, they exhibit many desirable traits compared to their micron-scale counterparts. Many of the improvements resulting from the decreased particle size are due to an increase in specific surface area [24, 26, 34]. Particles on the order of tens of nanometers have nearly as many atoms on the surface of the particle as in the center of the particle, allowing them to react and propagate quickly [33].

Nanoscale metal particles often exhibit unique physical characteristics that differ from similar micron-scale particles. These characteristics include unique magnetic and optoelectronic properties [33] and lower melting and ignition temperatures [13, 30]. Nanothermites exhibit several desirable improvements over micron reactants including lower ignition temperatures and faster propagation, up to many orders of magnitude faster than similar micron reactants [1]. The benefit of decreasing reactant particle size reaches a point of diminishing returns caused by an inert oxide shell present on most metal fuels. For example, a typical aluminum particle has a 3 nm thick oxide shell. On the micron-scale this oxide shell is not important, as it accounts for less than 0.1% of the total mass of a 50  $\mu\text{m}$  particle. However, as the particle size decreases, this oxide shell becomes a significant portion of the total mass. For a 50 nm particle, this oxide shell accounts for 32% of the total mass. Ideally, this oxide shell could either be eliminated or replaced with an energetic alternative. Recent work has explored these possibilities but a widely adopted method has not yet been established [9, 29].

## 1.2 *A Brief History of Welding and Joining With Thermites*

Hans Goldschmidt also pioneered the use of thermites for welding. Goldschmidt realized the potential of thermite reactions to generate molten metal and impart large amounts of heat to the surrounding material. Furthermore, the thermite reaction is self-contained, needing little to no outside energy. Goldschmidt recognized the potential application in construction and filed an additional patent for the use of thermites to weld streetcar tracks in 1903 [18]. This process proved to be so simple, inexpensive, and reliable that it is still widely used in the rail industry today [23]. Although the mechanism to weld steel with aluminum and iron oxide is well established, current work continues to improve on this mechanism. Recent research indicates the bond can be strengthened by combining the energy release of the thermite reaction with the alloying of aluminum and nickel [28].

### 1.2.1 *Joining Ceramics and Non-Metals*

Extensive work has been performed to investigate and understand glass-to-glass and glass-to-metal bonding [3, 4, 31]. Research efforts have demonstrated the ability to bond glass to iron, silver, gold, and copper, as well as many other metals and alloys [10]. Glass has been bonded to the surface of metals to prevent wear caused by acid, abrasion, and oxidation since ancient Egyptian times. Glass coatings are still widely used in turbines and printed circuit boards [10]. One type of glass to metal bonding is mechanical bonding. Two proposed mechanisms, dendrite and electrolytic, postulate

that the rough surface of the metal substrate allows the glass to flow and form an interlocking structure. The dendrite mechanism suggests metallic dendrites form in the glass during the reaction between the oxygen in the glass and the metallic element [21]. This is shown in Equation 1.2 for a reaction between cobalt monoxide and iron, reproduced from [10].



The electrolytic mechanism postulates the rough surface is the result of a corrosion mechanism [39]. This mechanism builds on the reaction proposed in the dendrite mechanism, but adds two additional steps. The additional reaction steps are shown in Equations 1.3, 1.4, and 1.5 , reproduced from [10].



It is believed this mechanism promotes the dissolution between the glass and metal, forming an interlocked key structure at the interface.

Another method of glass-to-metal bonding is chemical bonding. This method proposes a transition region between the bulk glass and the bulk metal where the mixing of the two species occurs [25, 42]. Unlike mechanical bonding, this region is homogeneous and the strength comes from chemical bonds, rather than key or dovetail type mechanical joints. These glass to metal bonds generally occur by adhesion chemistry between the metal oxide and the glass surface [10]. In the most

simple case, a metal oxide forms on the metal surface by a redox reaction with the glass. Then, the metal oxide diffuses into the glass surface, producing a region of intermixed glass and metal oxide. A similar process involves first doping the bulk glass with the corresponding metal oxide. When the interface is subjected to elevated temperatures, the highly mobile atoms diffuse between the two adjacent surfaces creating a region of equilibrium and resulting in a strong chemical bond [25].

When bonding dissimilar materials, matching the coefficient of thermal expansion is of paramount concern. Dissimilar coefficients induce unnecessary stress on the bond during heating. Glasses are often categorized in two categories: “soft” glasses, with low softening temperatures and large coefficients of thermal expansion, and “hard” glasses, with higher softening temperatures and lower coefficients of thermal expansion. Glass to glass bonds can be accomplished by using a third glass with a lower softening temperature. This “softer” glass is used much like a lead based solder in the joining of metals [10].

Ceramics and other non-metals are used widely in industry. In particular, there is increased interest in joining silicon wafers. The most common method of joining wafers is direct bonding. In direct bonding, also called silicon fusion bonding, the inherent tendency of clean, mirror polished surfaces to adhere to each other is enhanced when exposed to heat (in excess of 1000 K) and pressure [37]. A derivative of direct bonding called anodic bonding, uses large voltages (500 V) to bond silicon to sodium rich glass materials such as Pyrex [8]. Anodic bonding allows the sub-

strates to remain several hundred degrees cooler than traditional direct bonding. Two wafers, one with a sputter deposited coating of Pyrex, are heated to a temperature close to 700 K. A voltage of roughly 50 V is applied to join the wafers. One possible limitation of anodic bonding is its inability to bond materials with a silicon dioxide layer. Recent work attempts to extend the usefulness of direct bonding by investigating near room temperature joining using the gold/silicon eutectic [45] and processing in ultrahigh vacuum [19]. All of the previously introduced methods require a surface roughness of approximately 1 nm.

Some non-metals require special considerations when bonding, such as an external bonding agent in addition to an energy source. Some progress has been made using independent heat sources and bonding agents. In these bonds, the surface is typically media blasted. A layer of solder is then sputter-deposited and the surface is machined flat. A multilayer nanofilm, capable of generating heat through an alloying reaction, is placed between the prepared surfaces as a heat source [5]. Although this approach has been proven effective, it requires extensive pre-processing and its use is limited to substrates sturdy enough to withstand the necessary preprocessing. Additionally, nanofilms are typically manufactured in solid sheets and must be individually cut to the desired shape.



### 1.2.2 *Welding and Joining With Nanomaterials*

Investigations into welding and joining with nanomaterials is very much a new frontier. Several recent studies have investigated their use in specific applications, but the fundamentals are still being established. One of the most promising methods utilizes energy release through the alloying reaction of aluminum and another metal as discussed previously in Section 1.2.1. This alloying reaction uses multilayer metal foils to provide heat for welding, soldering, and brazing metals and select metallic glasses [41].

Recent research has shown promise in the joining of dissimilar materials through the use of disks comprised of nanothermite compositions of Al-NiO-Cu mixed to a stoichiometric ratio of 4 [2]. In his work, Zanjani utilized disks with a diameter of 3 mm and a thickness of 0.7 mm. The disks were used to join copper wires to glass substrates. The system was heated to approximately 700 K to initiate a thermite reaction. Although it is shown the bond was capable of supporting a glass substrate of around 3-5 g, extensive strength testing was not conducted. Furthermore, this study relied on an additional heat source (external to the thermite reaction) to elevate the system temperature.

Nanomaterials have also been used to join copper wires. This method of joining makes use of a paste composed of water and silver nanowires. One advantage of this technique is the ability to keep the bulk material at room temperature. This

method is able to exclude organic compounds during bonding, forming ultra-low resistance bonds [32].

The majority of the methods discussed require extensive preprocessing in tightly controlled environments and have limited utility. We aim to extend Goldschmidt’s idea of a simple and universal thermite bonding mechanism to modern applications. The development of a single “ink”, containing both a heat source and a bonding agent, would be ideal in many of these applications. This ink could be easily and accurately deposited on many types of surfaces and would ignite readily and react quickly. This reaction would provide adequate heat to promote bonding and would be accurate enough to bond only the desired areas. The ink would be composed of the heat source (the thermite) and the bonding agent (the diluent). The addition of diluents to thermites is a demonstrated concept. Thermite additives are widely used in the pyrotechnics industry [27] and are also used to perturb the thermite reaction to study the effects on propagation and reaction rate [15, 27, 36].

### *1.3 Bonding Criteria*

Traditional metal bonds are formed by creating a continuation of the substrate material. Here, we consider a different type of bond. This bond, a “sandwiched bond,” consists of a bulk bonding material ‘sandwiched’ between the substrate material on either side, as seen in Figure 1.2. Although this approach to bonding does not provide the advantage of a continuous material, it allows for the bonding of materials

that would otherwise prove very difficult. Furthermore, after the bulk bonding mechanism and ink formulations have been established, the bonding ink can be used in many different applications with only minor modifications to optimize heat transfer to the substrate material and promote bonding. With these properties understood for several materials, dissimilar material bonding will be very straightforward. We propose four criteria for the successful bonding of two substrates:

1. A reactant system must not be chosen from the systems known to produce gas at the adiabatic flame temperature or in final products.
2. A reactant system must have tailored heat release rate and quantity to the specific substrates being bonded.
3. The product species must have a continuous bonding agent network throughout.
4. The system must have a mechanism to bond to the substrates being bonded.

The first proposed criterion is the production of little to no gaseous species. A large percentage of gas negatively impacts the bonding mechanism in two ways. First, the expansion of gas in a confined area imposes unnecessary stress on the substrates, potentially compromising the material strength by either cracking or completely shattering the substrate. More importantly, gas generated within the reacting material expands quickly, often forcing the surrounding material outside of the desired bonding area. Some of the gas may also condense, depositing metal outside of the bonding area as discussed later in Section 3.3.

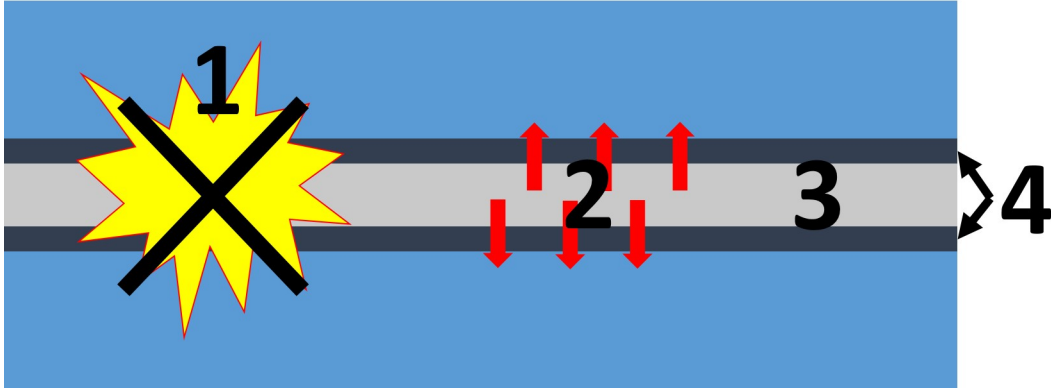


*Fig. 1.2:* Diagram of proposed bonding system requirements: 1) little to no gas generation, 2) tailored heat transfer characteristics, 3) continuous bonding structure, 4) substrate/bonding binding.

The second proposed criterion is the ability to tailor the heat transfer characteristics to the specific substrates being bonded. Depending on the substrate material, different heat transfer characteristics may be required. In the case of soda-lime glass, little to no heat transfer is desired as an excess of energy leads to thermal fractures along the surface. In contrast, bulk metallic substrates are not nearly as brittle and may tolerate, or even require, a larger amount of heat transfer. These heat transfer characteristics must be able to be tailored with regards to the both the amount of heat released and the rate at which it is released. These characteristics correspond to total enthalpy and burning time. One established advantage of nanothermite and nanofoil bonding is the ability to direct a large amount of energy to only the surface of a substrate. These methods allow a thin region near the surface to become thermally mobile enough to alloy and bond, while maintaining safe temperatures

throughout the remaining substrate.

The third proposed criterion is the formation of a continuously interlaced bond after the reaction has propagated. In an ideal bonding scenario, a completely dense bonded region would form, providing maximum strength and conductivity across the bond. To create this dense region, the bonding agent must be present in adequate quantities to fill voids between the substrate materials. Additionally, the bonding agent should have a low melting temperature to ensure adequate mobility and reduce the amount of heat lost to the bonding agent during the reaction. After the reaction front has propagated, the bonding agent must form a continuous structure between both substrates and along the length of the bond. Finally, the bonding agent must have adequate strength once bonded to withstand stresses placed on the material.

The fourth proposed criterion is an adhesion mechanism between the bonding mixture and the substrate's surface. Some substrates, such as copper and printed circuit boards (PCBs), readily adhere to potential bonding agents (such as tin) and easily provide a bonding force between the substrate and bulk bonding material. Other substrates, such as soda-lime glass and bulk silicon, require an additional mechanism to promote adhesion between the bulk bonding material and the substrate surface. This adhesion mechanism can take the form of an alloying reaction between a component in the bonding mixture and the substrate's surface.

## Chapter 2: Methods

This work focuses on the bonding of soda-lime glass substrates. The primary motivation for this was the easy availability of flat substrates at low cost, and the ability to image through the substrate. Microscope slides, purchased from a local chemistry supply store, were used as the substrates in this study. The transparent nature of soda-lime glass facilitated optical combustion velocity measurements through the adjacent substrate. Additionally, it allowed for visual inspection of the bonded joint. Soda-lime glass substrates are naturally flat allowing for even deposition of the ink and ensuring good contact with the substrate surface. Although several other substrates, such as silicon, are of great interest to the scientific community, this work aims to provide a framework for aluminum nanoenergetic based bonding inks that can be modified for many applications.

Aluminum nanoparticles with an 80 nm diameter were purchased from Novacentrix for use as the metal fuel. Aluminum is a popular choice for fuel given the stability of alumina, the corresponding oxide, its low cost, and high combustion enthalpy. Thermogravimetric analysis of the bulk aluminum indicated that it contained 64% reactive aluminum and 36% inert alumina by mass. Tungsten (VI) oxide (tungsten

trioxide,  $\text{WO}_3$ ) with a 100 nm diameter was purchased from Sigma-Aldrich and used as the the oxidizer. Tungsten trioxide produces relatively little gaseous species while maintaining a high adiabatic temperature and reasonable enthalpy. Tin was chosen as the bonding agent due to its low melting temperature and latent heat of fusion. The low melting temperature allows the tin to easily flow and form continuous morphologies while the low latent heat of fusion means the tin has a minimal thermal load on the reacting system. Tin requires only 4% of the energy per mass to melt compared to silicon. Tin with a diameter of 100 nm was purchased from Sigma-Aldrich and used as the bonding agent in this study. These selections are summarized in Table 2.1.

*Tab. 2.1: Summary of reactant properties.*

Item	Purpose	Size	Manufacturer
Aluminum	Fuel	80 nm	Novacentrix
Tungsten Trioxide	Oxidizer	<100 nm	Sigma-Aldrich
Tin	Bonding Agent	<100 nm	Sigma-Aldrich

## *2.1 Pressure Cell Measurements and Thermochemical Modeling*

The effect of the tin diluent on the nanothermite reaction is investigated through constant volume combustion experiments. Pressure and optical signals are simultaneously recorded during the combustion of a known amount of sample in a constant volume chamber. The experimental setup is identical to that used by Sullivan, the

diagram is reproduced in Figure 2.1 [40]. The experiments maintained a constant 25 mg of  $\text{Al}/\text{WO}_3$  (the nanothermite) in stoichiometric proportions. Tin particles, the bonding agent, are added to the 25 mg of nanothermite to examine the effect on combustion. The amount of the bonding agent is given as a percentage of added weight with respect to the base mass of nanothermite.

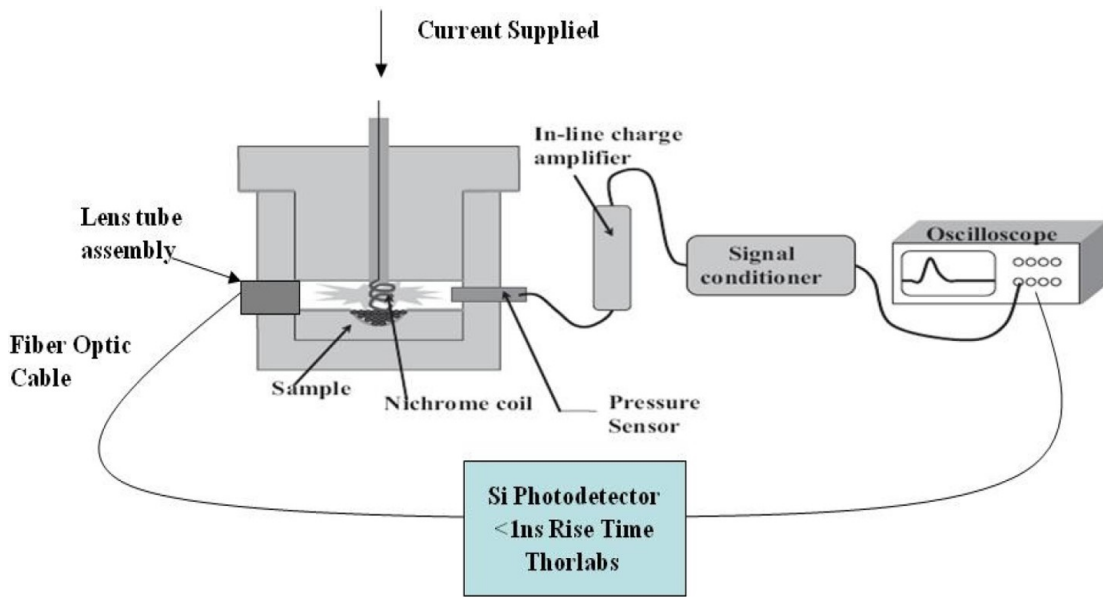


Fig. 2.1: Diagram of constant volume experiment, reproduced from [40].

The total mass during these tests increased as the percentage of added tin increased. For the case of 50% added tin, the mixture is comprised of 5.6 mg aluminum (64% active), 18.4 mg tungsten trioxide, and 12.5 mg tin for a total mass of 37.5 mg and a specific volume of  $0.00288 \text{ g}/\text{cm}^3$ . The total mass of the sample in the constant  $13 \text{ cm}^3$  combustion chamber increases with the addition of tin while maintaining a constant mass of nanothermite. Samples combined in glass vials with hexanes are



mixed in an ultrasonic bath for thirty minutes before air drying. Large agglomerations are broken up with a spatula before using the dry powder. Constant volume equilibrium calculations are made using the Cheetah thermochemical equilibrium code with the JCZS library [22]. These calculations use the same specific volume as the experimental values.

## 2.2 *Deposition*

This bonding technique depends greatly on a reliable deposition method. The ideal deposition would be consistent, customizable, and yield thin lines. It is also desirable for deposition to occur as quickly as possible to maintain a homogeneous ink. The deposition process needs to yield a homogeneous fuel/oxidizer bonding agent regardless of thickness. Special considerations need to be made when dealing with materials of varying densities or size, as denser particles are more likely to settle out of the deposition ink, resulting in a heterogeneous deposition. Additionally, consistent results are desired regardless of substrate. With these requirements in mind, two deposition approaches are evaluated: electrospray and direct write.

### 2.2.1 *Electrospray*

Electrospray produces fine droplets from a liquid precursor by applying an electric field. The liquid precursor in the needle is drawn to a point until the concentration of charge forces the formation of a jet at the tip. The small particles produced

continue to shrink as the solvent evaporates. Eventually, the surface charge once again forces the particle to fragment creating an expanding cone of dispersed particles. The major benefit of electrospray in this application is the inherent ability to produce dry depositions. By depositing dry material, surface tension is eliminated along with the drying effects which plague wet deposition techniques. Dry deposition also prevents particles from selectively settling out during the drying stage.

Two problems become apparent when considering electrospray as a potential deposition technique: the desire for accurate, thin lines and the need to deposit on a variety of substrates - both conductive and insulative. One solution to these problems is the use of a metal mask. The electric field can be generated between the needle and mask allowing for a consistent spray, regardless of the conductivity of the substrate. Additionally, the mask produces a consistent line width. Unfortunately, two issues arise while using a conductive mask. First, the mask walls exhibit a shadowing effect along the edges of the line (near the mask walls) where the charged particles are attracted to the oppositely charged wall. This shadowing effect is exasperated as the line increases in thickness or decreases in width.

Second, in order to produce a uniform layer of material across the width of the line, the diameter of the spray must be 4-5 times the desired width. The need for a much larger spray diameter greatly reduces the rate at which material can be deposited, as the mass flow rate through the mask to the substrate is only a fraction of the actual mass flow rate. This effect can be offset by increasing the mass loading of the

ink. However, a solids loading over  $100 \text{ mg/ml}$  is not practical, as the suspension of particles becomes problematic. The additional mass of nanothermite on the mask surface is also a safety concern. In general, the quantity of dry thermitite being handled should be reduced to the minimal necessary. This safety concern is worsened by the presence of a high voltage creating the possibility of arcing to the mask and igniting the material.

Another possibility to address the issues with electrospray is through the use of an aperture ring. An aperture ring is a conductive ring placed between the needle and the substrate. An electric field is applied between the needle and ring in order to provide the necessary electric field and drive the electrospray process (as in a conventional setup). The ring serves two purposes in this application. First, the electric field is applied between the needle and the aperture ring eliminating the need for the substrate to be conductive. Second, the aperture ring increases the near-field region of the spray geometry allowing for a more accurate and confined deposition. Generally, a narrow diameter spray requires a lower mass flow rate. Although there is no longer a shadowing effect or an excess of material, as seen in the masking approach, the low mass flow rates make the deposition time prohibitively long. Duan et al. developed a process to produce narrow lines by operating in the near field range of the spray [12]. They employed a volumetric flow rate of  $0.2 \text{ ml/h}$  with a solids loading of  $100 \text{ mg/ml}$ . Using these parameters, it would take 60 minutes to deposit a single line of ink on a microscope slide. This long deposition time is particularly problematic when using unstable inks as the particles may fall out of

suspension during the deposition process.

### 2.2.2 *Direct Write*

Direct write is an additive manufacturing technique in which a stage and deposition nozzle are moved in relationship to each other while the deposition nozzle discharges material. Controlling the X-Y-Z location of deposition as well as the rate of material deposition allows complex three-dimensional geometries to be fabricated. Two types of direct write were explored: automated direct write and manual direct write.

The automated direct write system utilized a modified MakerBot Replicator fused deposition modeling (FDM) platform. Each of the FDM nozzles was replaced with a pneumatically driven 5 cm<sup>3</sup> syringe. When material was not being deposited, a negative pressure was applied to the syringes to produce bubbles and facilitate constant mixing. Although the solutions needed to be stable for several minutes on their own, the bubbling allowed for the use of a wider range of solutions. The direct write process proved to be quick and reproducible. However, many problems arose as a result of the wet deposition, including the presence of surface tension which forced the lines into a nonuniform geometry during drying.

A simplified version of direct write is manual direct write deposition. To create uniform line widths and straight edges, a mask is used. Blue masking-tape is applied to clean, dry slides and a relief is cut through the center. The ink is deposited with a micropipette and allowed to flow and fill the relief. Once the solvent has

evaporated, the process is repeated to gradually build layers of material. Although this method is more crude than the previously discussed methods, it still provides consistent layer thicknesses and profiles.

This work used a manual direct write deposition method. This allowed more focus to be placed on formulating inks and understanding the nanothermite/bonding agent mechanism, rather than refining deposition techniques. Line reliefs were chosen to be approximately 3 mm wide by 75 mm long. This geometry ensured the thickness of the lines (between 10  $\mu\text{m}$  and 150  $\mu\text{m}$ ) was an order of magnitude less than the next smallest dimension. This allowed the problem to be considered one dimensional. Inks were prepared at a concentration of 100  $\text{mg}/\text{ml}$ . The total solids loading changed with the addition of tin. However, the solids loading of aluminum tungsten trioxide was held constant. In these experiments, it was of more importance that the concentration of thermite be kept constant than the overall solids loading.

This approach utilized the experimental setup described in Section 2.1. Isopropal alcohol was chosen as the solvent because of its polar nature, which allows powders of varying densities to be held in suspension. The inks were mixed in an ultrasonic bath for thirty minutes, breaking up agglomerations to achieve a uniform state. The ink was extracted and deposited on the glass slides with a micropipette while the vial remained in the ultrasonic bath. The water was changed regularly to maintain near room temperature. The solvent was allowed to evaporate off the slide between depositions. This process was repeated until the desired number of layers had been

deposited.

After the final layer was deposited, the slides were dried for several hours at room temperature, to ensure all of the solvent had evaporated, before the masks were removed. The slides were weighed before and after deposition to determine the mass of material deposited. The line profiles were examined using a Tencor Alpha Step 200 profilometer to determine line geometry and thickness. Although line thickness varied slightly along the length of the lines as well as between slides with the same number of layers, the average line thickness and amount of material deposited increased as the number of deposition layers increased. This can be seen in Figure 2.2. By design, the line width remained constant regardless of thickness.

The ideal line profile has a flat top and straight walls with ninety degree corners, as shown in Figure 2.3. This profile has the most contact area when sandwiched with an adjacent line of the same profile. Less optimal is the line with a rounded top, shown in Figure 2.4. The most common error seen in the line profile produced by manual direct write deposition is a valley in the center of the line. This is the result of the accidental dragging of the micropipette down the center of the line during deposition. It is seen more frequently in lines with a higher number of deposited layers. The material from this channel is either pushed to one side (as seen in Figure 2.5) or removed by the micropipette tip leaving a relatively flat top profile (as shown in Figure 2.6). Despite a variation in profile, the combustion velocity does not noticeably fluctuate. Even in the presence of these channels, the width of

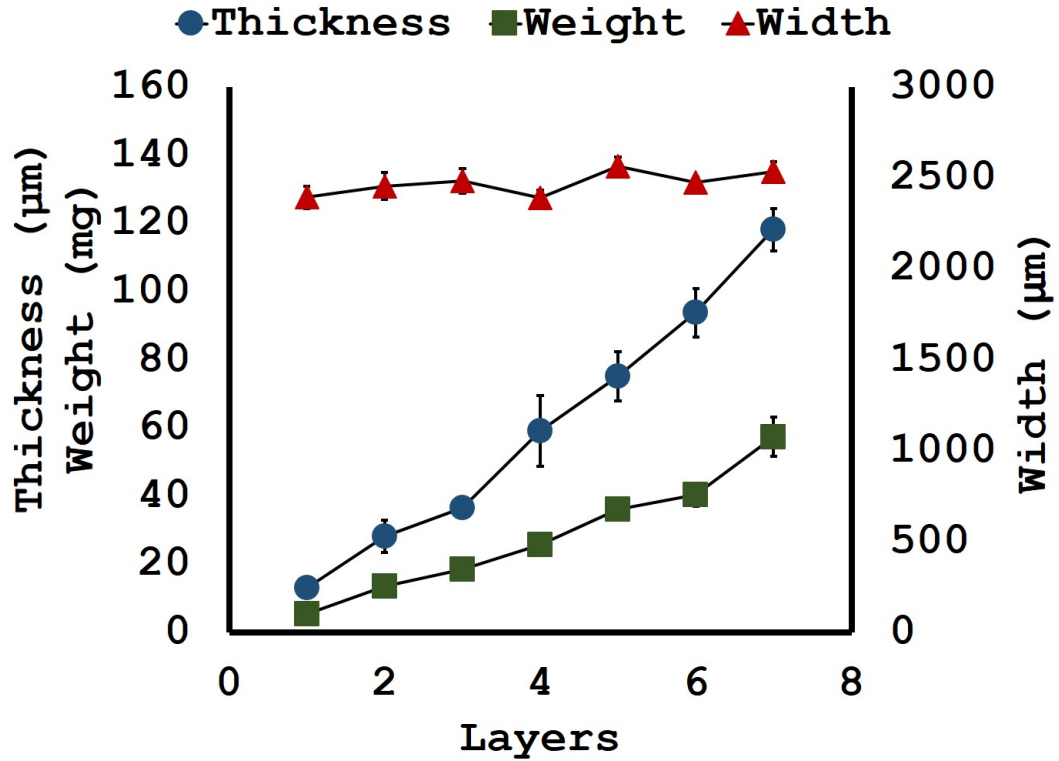


Fig. 2.2: Number of layers vs. total weight, thickness, and width.

the line is roughly 10 times the thickness of the line, leaving the line thickness (the smallest dimension) as the controlling dimension.

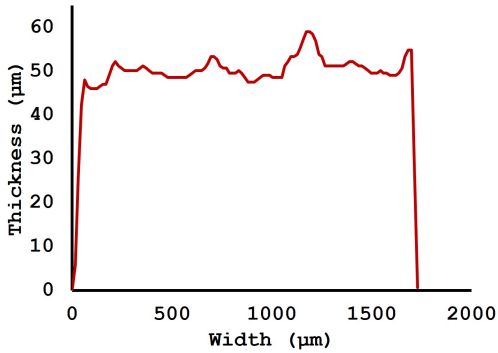


Fig. 2.3: Profile of ideal line

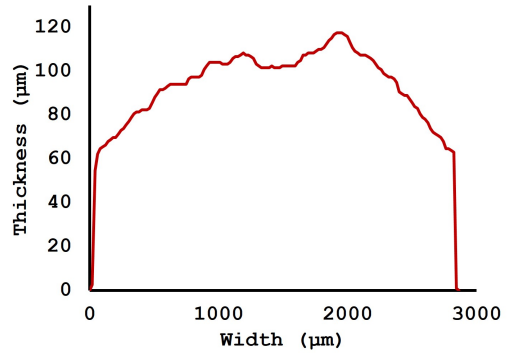


Fig. 2.4: Profile of rounded line

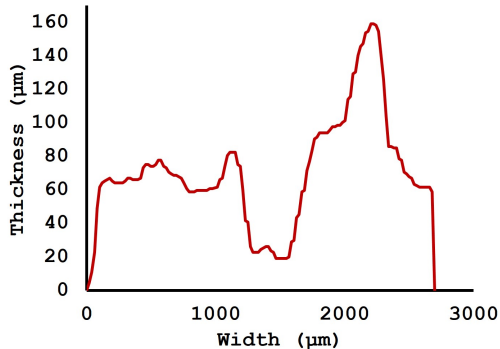


Fig. 2.5: Profile of line with channel and material pushed to side

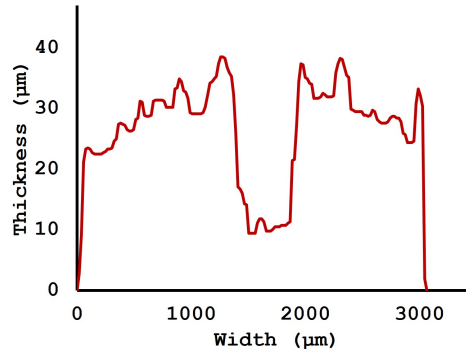


Fig. 2.6: Profile of line with channel and flat top

### 2.3 Combustion Velocity

Line combustion velocities were measured with high speed video using a Phantom V12.1 camera. Combustion velocities were measured both with the line open to the atmosphere on three sides and sandwiched between two soda-lime glass substrates. Slides were prepared as discussed in Section 2.2. Two slides with similar line thickness were sandwiched together with the lines facing each other. The slides were positioned such that half of each slide was left exposed and half was in contact with the adjacent slide.

Two spring loaded clamps (one on either side of the line) apply a total force of approximately 127 N to the substrates along the length of the line. It is important the clamps apply a constant pressure throughout the duration of ignition and burning to ensure the substrates remain in intimate contact with each other during the reaction. The slides are positioned with the line face perpendicular to the camera lens.



The lines were ignited by a small piece of resistively-heated wire with pure Al/WO<sub>3</sub>. A shield around the ignitor was used to restrict ignition to a several millimeter area of the desired line. Figure 2.7 shows the experimental setup as viewed by the camera. For each test, three independent measurements were taken: the unconfined speed of line A, the confined speed of line A plus line B, and the unconfined speed of line B. Although the first line is observed by looking at the top of the deposited line and the second line is observed through the glass slide at the bottom of the line, a difference in combustion velocity was not observed. Measurements were made for each of the three regions using a position vs. time calculation for the entire length of the line.

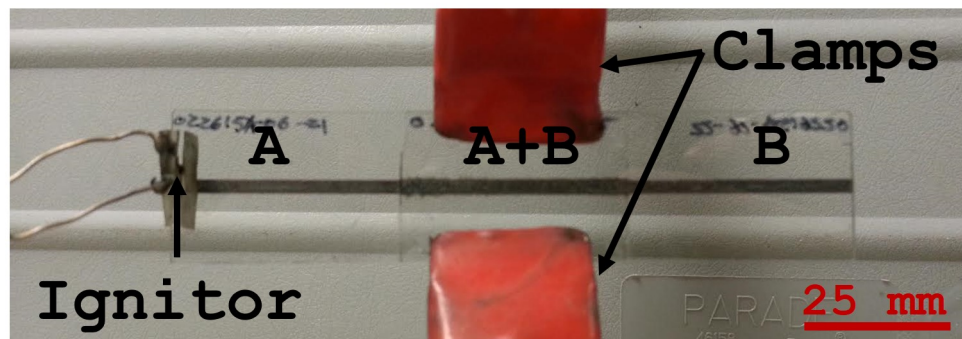


Fig. 2.7: Burn speed experimental setup as viewed by the camera.

## 2.4 Bond Strength

The shear strength of the bonded slides is also of interest. To evaluate this, a simple one-dimensional stress test was developed. This test loaded the bonded slides parallel to the inked line. This loading scenario resulted in the determination of the shear strength of the bond, expressed as  $\tau = \frac{F}{A}$ . Here  $F$  is the force and  $A$  is the area. A diagram of the experimental setup is shown in Figure 2.8.

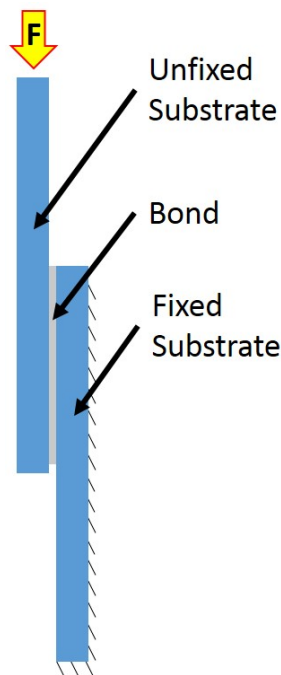


Fig. 2.8: Diagram of stress test.

The fixed substrate is secured to a stationary base while a loading sleeve is placed over the top of the unfixed substrate. This loading sleeve is constrained to movement along the length of the deposited lines. The sleeve is attached to an empty bucket

and water is added in a constant stream at approximately 1 liter per minute to gradually load the system. The slide is loaded until a failure is observed (i.e., the bond breaks) and the final weight of the bucket is measured with an American Weigh hanging scale ( $110 \times 0.05$  lbs). The shear strength is calculated and the testing apparatus is reset.

## Chapter 3: Results

### *3.1 Pressure Cell Measurements and Thermochemical Modeling*

The experimental pressure and optical signals are collected and the maximums are compared with the calculated values. Examples of these recorded signals for 0% and 100% added tin are shown in Figures 3.1 and 3.2. Among the values generated by thermochemical equilibrium calculations, several trends should be noted. First, the temperature decreases sharply with respect to the pure thermite value before plateauing and remaining relatively constant as seen in Figure 3.3. This initial temperature decrease corresponds to a loss of sensible energy as the tin vaporizes. As the percentage of tin increases, the reaction no longer generates enough energy to vaporize all the tin and the temperature remains at the boiling temperature of tin. Secondly, peak pressure increases sharply and is maximized at 30% added tin. As added tin increases beyond this point, peak pressure declines at roughly the same rate. The peak pressure (at 30% added tin) corresponds with the leveling off of temperature. This correlates with the transition from gaseous tin species to liquid tin species. We conclude this inflection point corresponds with the fastest reaction rate. Cheetah predicts that added tin beyond 100% (corresponding to equal parts tin and nanothermite) will thermally quench the reaction and fails to converge at

an equilibrium solution.

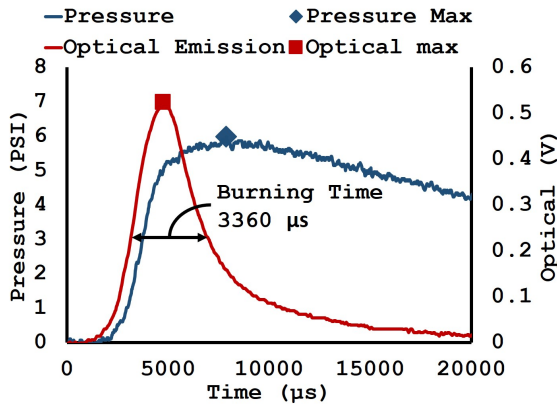


Fig. 3.1: Pressure and optical signals for combustion of pure Al/WO<sub>3</sub>

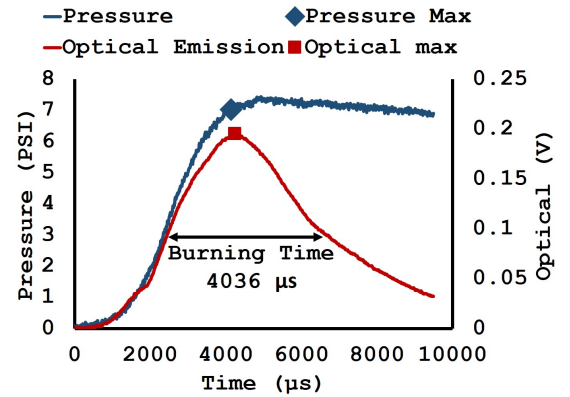


Fig. 3.2: Pressure and optical signals for combustion of Al/WO<sub>3</sub> + 100% tin

This relationship is not observed in the experimental pressure measurements. The experimental and calculated peak pressures are normalized by the peak pressure of pure Al/WO<sub>3</sub> and shown in Figure 3.3. Since we are more concerned with the overall trends and relationship between experimental and calculated, this scaling more adequately captures the features of interest. When added tin is between 0% and 30%, peak pressure is expected to rise rapidly. However, in the experimental data it appears to remain roughly constant. Similarly, beyond 30% added tin, peak pressure is expected to decrease, but is observed rising slightly and then remaining constant. Additionally, the observed peak pressure remained elevated, relative to the pure Al/WO<sub>3</sub> system, for even large amounts of added tin. For small amounts of added tin, the tin particles are in such low concentrations that they are likely clustered in groups rather than homogeneously mixed as expected in the equilibrium

calculation. The minimal gas generation does very little for the reaction as a whole because the tin is isolated in a limited number of locations. Although it is likely the tin remains in similar sized clusters irrespective of the amount added, these local tin pockets become more numerous as larger amounts of tin are added. Increasing the number of these pockets has a greater impact on the global reaction kinetics.

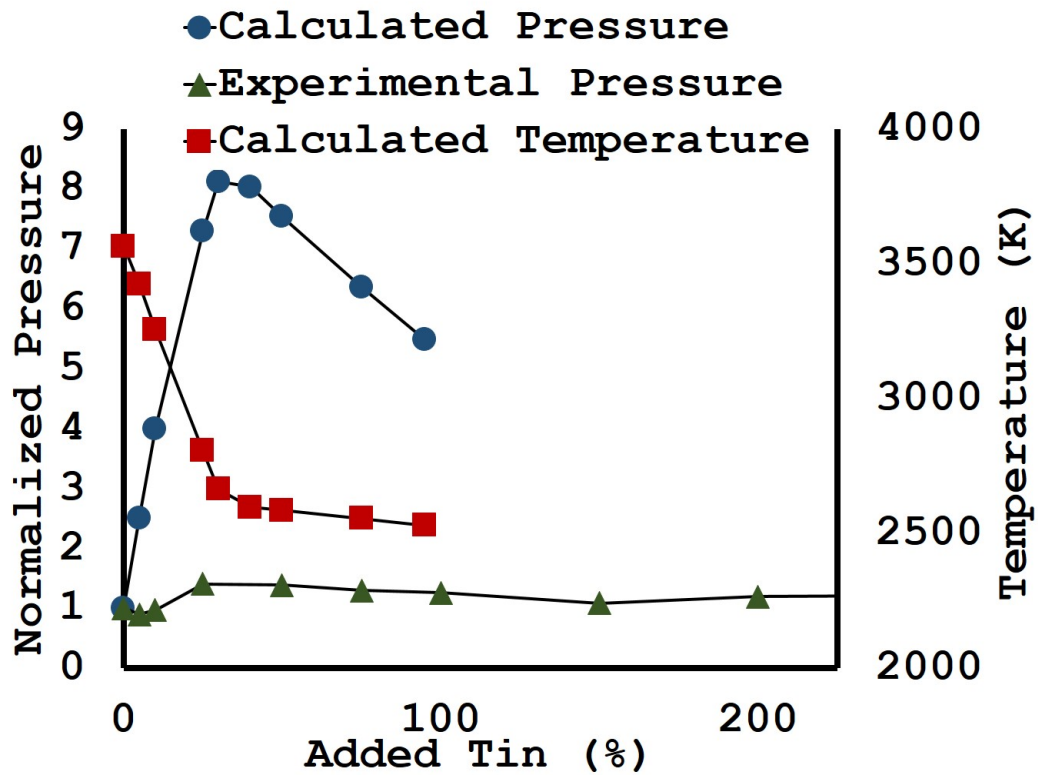


Fig. 3.3: Peak pressure magnitude (experimental and calculated) and adiabatic temperature (calculated) as a function of added tin.

Equilibrium calculations predict the reaction will become limited by the vaporization of tin as larger percentages are added. This is realized on an experimental level as well. Pure Al/WO<sub>3</sub> has a peak optical emission time well before the peak pressure.

This behavior is examined by Sullivan et al. and is indicative of a reaction where convective heat transfer is not the driving mechanism. Nanothermites with large quantities of gaseous species (e.g., aluminum/copper oxide) exhibit peak pressure either before or simultaneously as peak optical emission is achieved. To examine the gas release timing of this nanothermite and bonding agent mixture, the relationship between peak pressure time (PPT) and peak optical emission time (POT) is investigated with the ratio PPT/POT. Figure 3.4 shows this relationship for the experimental studies. Ratios greater than 1 indicate that peak pressure occurs *after* the peak optical signal. Ratios less than 1 correspond to peak pressure being achieved *before* peak optical emission. A ratio of 1 indicates the two are achieved simultaneously. Pure Al/WO<sub>3</sub> has a PPT/POT ratio of approximately 1.9. At 50% added tin, the average PPT/POT ratio approaches one and remains approximately one for increased amounts of added tin. As discussed previously, tin promotes gas generation and the addition of this easily vaporized tin will slowly force a PPT/POT ratio close to that of other gas-generating nanothermites. By examining Figures 3.1 and 3.2, it is evident the addition of tin reduces the PPT, while POT remains relatively constant. Additionally, the ratio approaches one asymptotically indicating that tin vaporization occurs with the bulk reaction rather than as a result of pre-heating.

Total burning time was defined as the time between the optical signal initially reaching 50% of the maximum intensity and when the signal eventually fell below 50% intensity after the peak as shown in Figures 3.1 and 3.2. Burning time was deter-

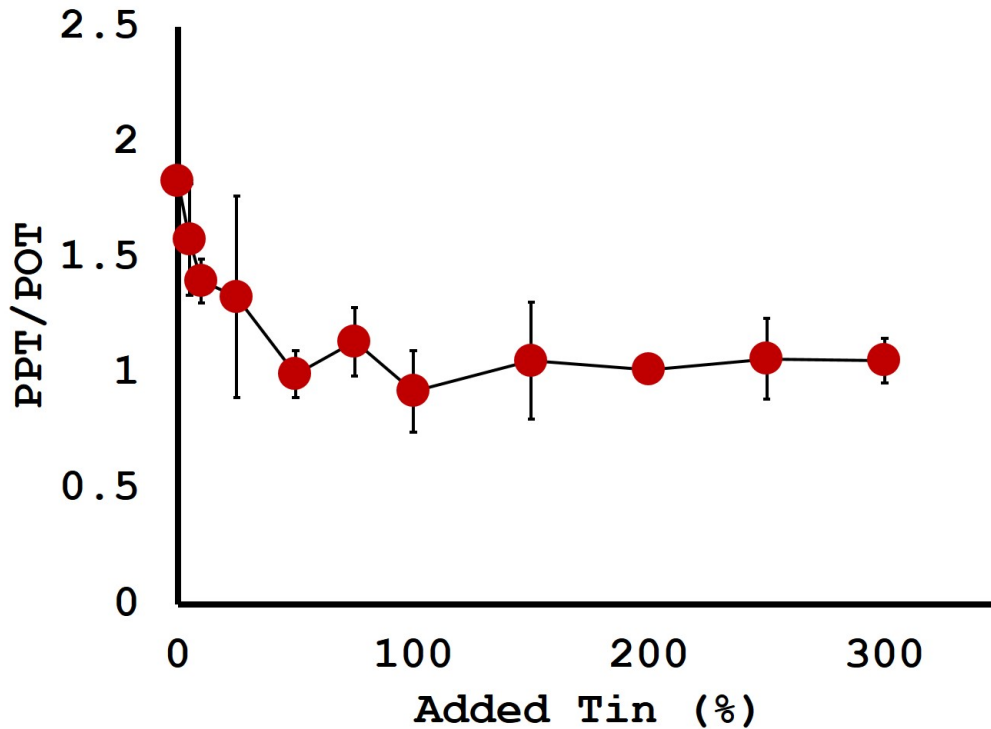


Fig. 3.4: Relationship between peak pressure time and peak optical time.

mined during pressure cell testing and is summarized in Figure 3.5. The pressure cell results show an initial increase in burning time for  $< 25\%$  added tin. At this point, there is a sharp decrease, reaching a minimum at or slightly after  $25\%$ . Burning time subsequently increases as tin is added. The sharp initial increase in burning time corresponds to the lack of a peak pressure increase seen for small percentages of tin in Figure 3.3. As discussed previously, the tin is most likely agglomerated in a few pockets, increasing the total thermal mass of the system and therefore burning time. However, the presence of this tin does little to change global reaction kinetics. The sharp decrease in total burning time aligns with the increase in peak pressure



observed around 25% added tin. For larger amounts of added tin, the burning time increases steadily. The added tin is likely adding so much thermal mass, it is limiting the reaction. Since it takes very little energy to fully melt tin, regardless of the amount added, it is likely that all the tin is melted and the vaporization of tin moderates the combustion velocity. This idea is supported with the plateau seen among experimental peak pressure measurements.

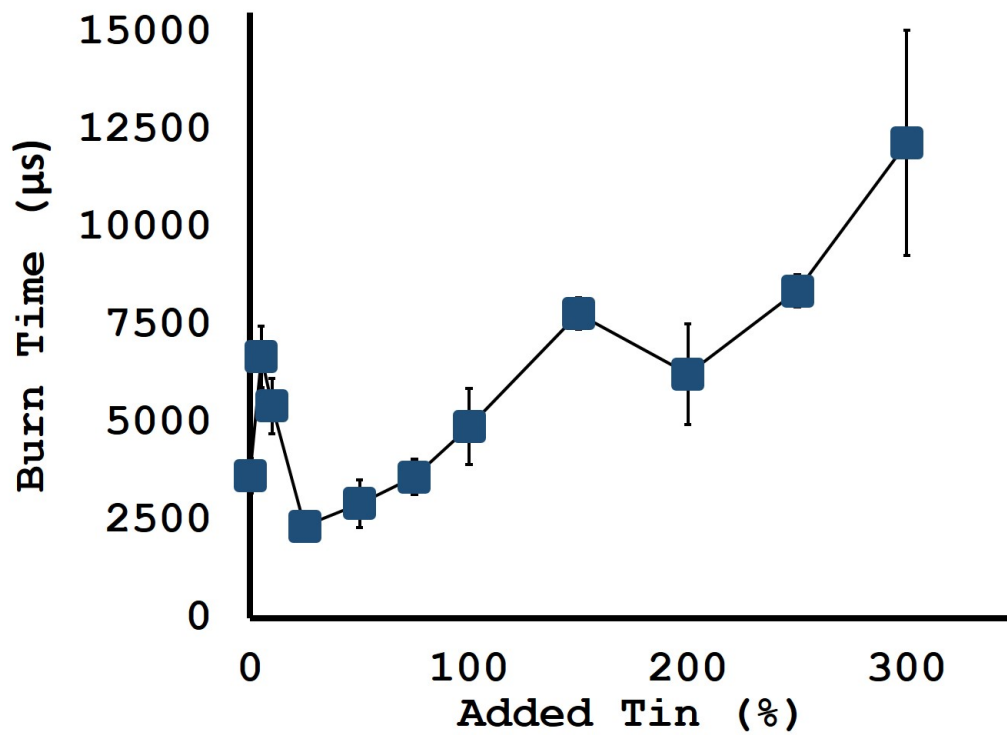


Fig. 3.5: Burning time as a function of added tin.

### 3.2 Combustion Velocity Results

The combustion velocity data, shown in Figure 3.6, relates line thickness to propagation velocity. This shows that the minimum thickness to propagate a reaction is nearly constant and not a function of the percentage of nanothermite in the total mass. Lines propagated selectively at a thickness of 15  $\mu\text{m}$  and propagated with a near 100% success rate by 25  $\mu\text{m}$ . The propagation rate of compositions of pure thermite (the blue line) and 50% added tin (the red line) increase initially with an increase in thickness. The combustion velocity for compositions containing 100% added tin (the yellow line) is relatively constant with regard to thickness. Compositions containing 50% or 100% added tin both exhibit an increase in gas generation compared to pure Al/WO<sub>3</sub>.

The data also indicate a thickness region where the combustion velocity of a composition with 50% added tin propagates faster than pure thermite. This region corresponds to an increased amount of gas generation that promotes convective heat transfer and results in faster combustion velocities. This thickness region also corresponds to the strongest bond as discussed later in Section 3.4. We note that for a constant thickness, the unconfined and confined burn speeds are identical. Adding an additional substrate (e.g., sandwiching the line between another glass slide) does not noticeably increase the minimum thickness required to achieve propagation. It is possible a small increase in minimum thickness is needed, but not observed due to the limited resolution available in these experiments.

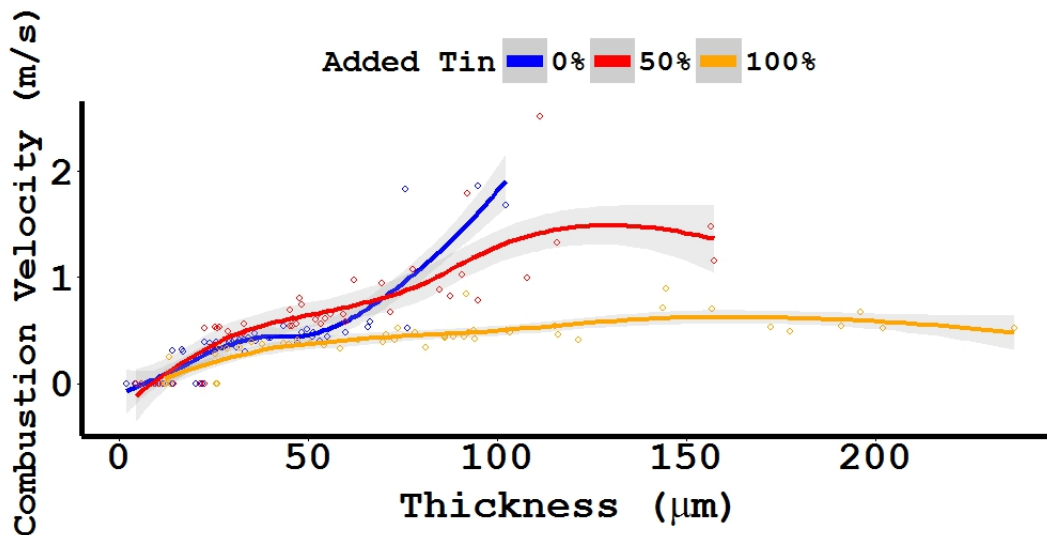
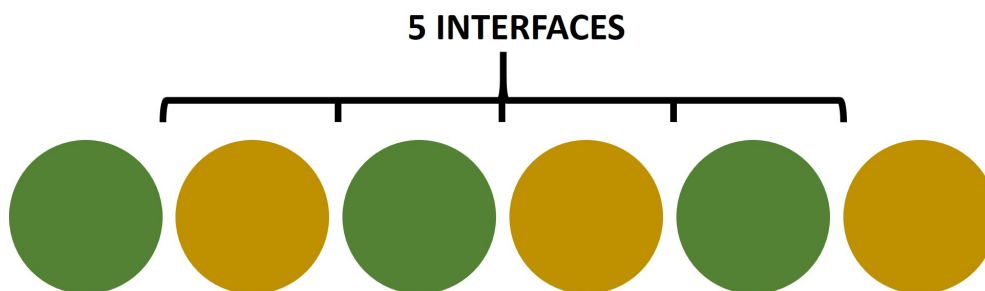


Fig. 3.6: Combustion velocity as a function of thickness for 0%, 50%, and 100% added tin.

Presumably the large percentage of tin in the 100% added tin samples hinders the kinetics of the reaction by decreasing the proximity of the fuel and oxidizer. It is well established nanothermite reactions rely heavily on homogeneous mixing and a large interface area between the fuel and oxidizer. When considering the pure thermitic case, with a constant particle size between all species, a stoichiometric mixture corresponds to 43% aluminum and 57% tungsten trioxide particles. These proportions change to 30% aluminum, 39% tungsten, and 31% tin for a 50% added tin sample. In the case of 100% added tin, there is 23% aluminum, 30% tungsten, and 47% tin. To achieve a more complete understanding of the possible kinetic impacts of a diluent particle, a simple simulation study was conducted. We consider the traditional scenario of sampling two different colors of balls from an urn without

replacement. Each ball represents a single species (either fuel or oxide) in the nanothermite system, where the initial probability of selection is proportional to the species representation in the Al/WO<sub>3</sub> system. The balls are exhaustively sampled and the number of interfaces (i.e., any instance where a fuel is sampled immediately before or after an oxide) is counted as shown in Figure 3.7.



*Fig. 3.7:* Interface diagram for an ideal six particle system.

Next, a percentage of diluent is added to the system and the simulation is repeated. The results of this simulation are shown in Figure 3.8, which relates the average percentage of interfaces to percentage of added tin. The percentage of interfaces is given as a proportion of an ideally mixed sample, like the one shown in Figure 3.7. An ideally mixed sample of a two species system would see one less interface than number of particles. In Figure 3.7 there are 5 interfaces for 6 particles. The number of interfaces between fuel and oxide particles decreases to only 25% of the ideal scenario and nearly half of its initial value for a sample with 100% added tin. Based on these results, it is expected a reaction which relies heavily on intimate mixing and a large interface area between fuel and oxidizer species will be negatively affected by

large percentages of diluent particles. Additionally, we examine the average string length of the diluent particle. The average length of the diluent particle is representative of the ability of the tin to flow and coalesce with adjacent particles. As the percentage of added tin increases, so does the the average length of the diluent particle string as seen in Figure 3.9. This corresponds with larger clusters of tin in the bonding agent mixture.

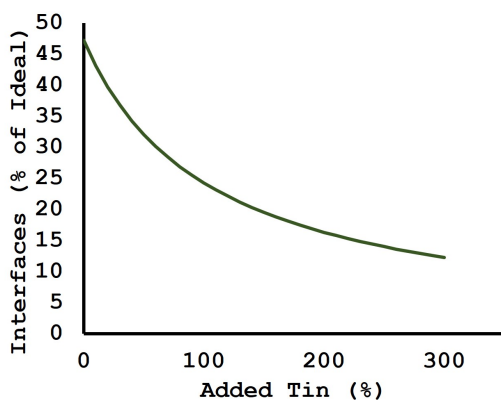


Fig. 3.8: Interfaces, as a percentage of ideal, vs. added tin.

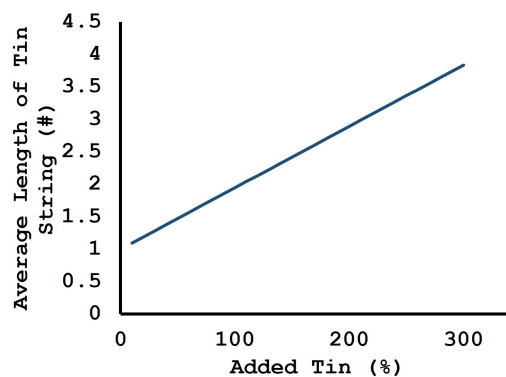
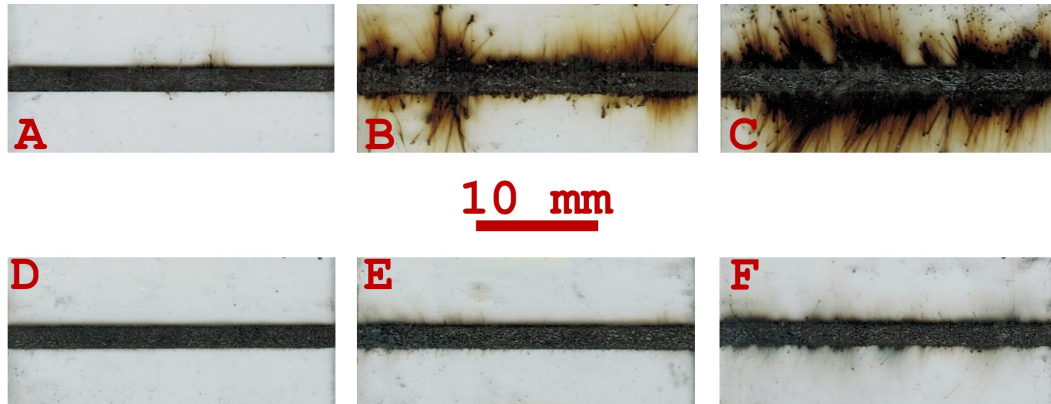


Fig. 3.9: Average length of tin string as a function of added tin.

### 3.3 Bonding

The first criterion for successful bonding is the reaction should produce little to no gaseous species. The justification for this criterion is given in Section 1.3. The experiments showed increased gas production as the amount of added tin and/or thickness increased. Both of these scenarios correspond to more tin in the system that is available to be vaporized. Figures 3.10 shows images of several slides after

combustion velocity testing. The ideal, well-bonded case corresponds to a small total mass of tin. The addition of tin, either by increasing the total amount of material or percentage added, drives gas production. Figure 3.10 A, B, and C show depositions of 50% added tin with thicknesses of 50  $\mu\text{m}$ , 75  $\mu\text{m}$ , and 100  $\mu\text{m}$  respectively. For comparison, pure Al/WO<sub>3</sub> with the same thicknesses of 50  $\mu\text{m}$ , 75  $\mu\text{m}$ , and 100  $\mu\text{m}$  respectively is shown in Figures D, E, and F. It is clear gas generated by tin in large amounts perturbs surrounding material and may create a gap in the continuous bonding agent structure.



*Fig. 3.10:* Figures of substrates post reaction. Figures A, B, and C are Al/WO<sub>3</sub>+50%Sn with thicknesses of approximately 50  $\mu\text{m}$ , 75  $\mu\text{m}$ , and 100  $\mu\text{m}$  respectively. Figures D, E, and F are pure Al/WO<sub>3</sub> with thicknesses of approximately 50  $\mu\text{m}$ , 75  $\mu\text{m}$ , and 100  $\mu\text{m}$  respectively.

Figure 3.11 depicts a scenario when excessive gas generation perturbed the surrounding material, leaving a several hundred micron hole in the bonding material structure.

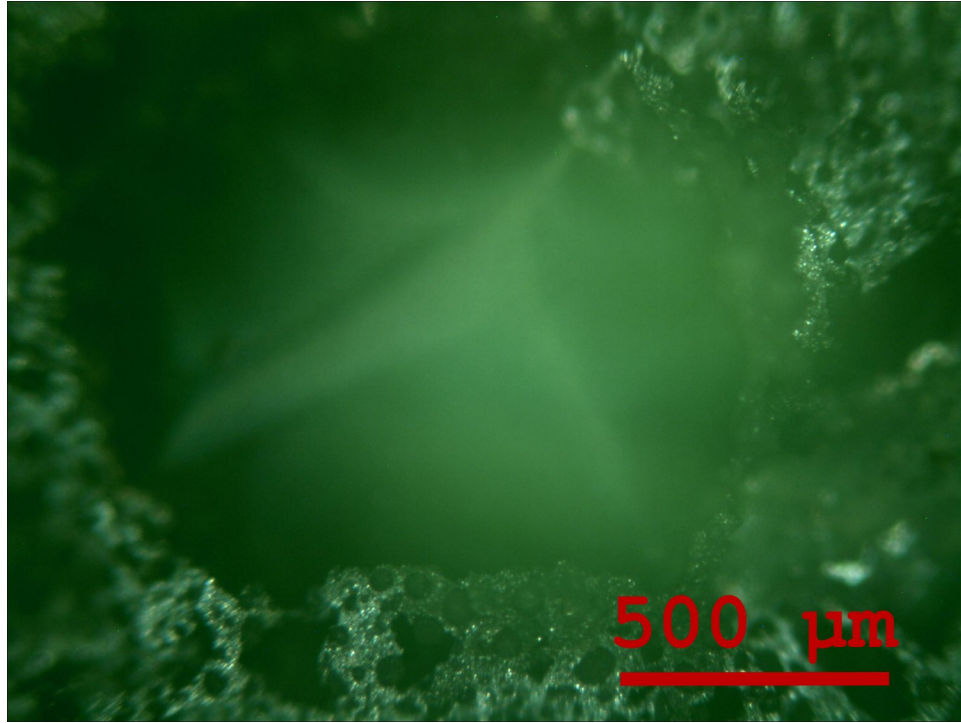


*Fig. 3.11:* Large hole in bonding material structure caused by excessive gas generation.

The second criterion is the ability to tailor energy transfer for a specific substrate. The main properties of interest are the depth at which a temperature increase will be seen in the substrate and the slope of the thermal profile in the substrate. Both of these properties can be investigated with basic thermodynamics. We will consider the case of steady state heat flux into the substrate using the maximum value of heat flux to establish an upper bound. This value is calculated by taking the total amount of energy released and dividing by the total experimental burning time. This assumption corresponds to a square wave of heat flux representing the reaction zone. Consequently, the ramp at the leading and trailing edges of the reaction zone will be lost. We will assume these portions of the reaction wave do not greatly effect

the average heat flux. Fourier's law, given in equation 3.2, indicates how the energy release rate effects thermal penetration. Here  $k$  is thermal conductivity,  $\dot{q}$  is heat flux, and  $T$  is temperature. The X direction is defined as into the substrate.

$$\frac{q}{t} = \frac{k(T_{hot} - T_{cold})}{\Delta X} \quad (3.1)$$

$$\Delta X = \frac{k\Delta T}{\dot{q}} \quad (3.2)$$

Equation 3.2 shows the relationship between temperature change and distance into the substrate. Since  $k$  can be considered relatively constant regardless of the percentage of added tin and the reaction temperature changes very little after 30% added tin, the only parameter changing is  $\dot{q}$ . The temperature change as a function of depth into the substrate for  $\dot{q} = 1.0E6 \frac{W}{m^2}$  and  $\dot{q} = 2.5E5 \frac{W}{m^2}$ , comparable to reactions containing 50% and 100% added tin respectively, are shown in Figure 3.12. Although no quantitative estimation of thermal penetration can be gathered from these equations because many assumptions and simplifications were made, a qualitative relationship between heat flux magnitudes and thermal profiles can be established. It is clear as the heat flux increases, the maximum distance into the substrate that a temperature increase is experienced will decrease.

Thermochemical equilibrium calculations show the amount of heat release can be modified by increasing the amount of tin in the reaction. Although this seems counterintuitive since a diluent is being added to the system, the tin acts as a secondary fuel and oxidizes with available oxygen. Total energy release increases to a maximum at 30% added tin and then decreases, as shown in Figure 3.13 for thermochemical



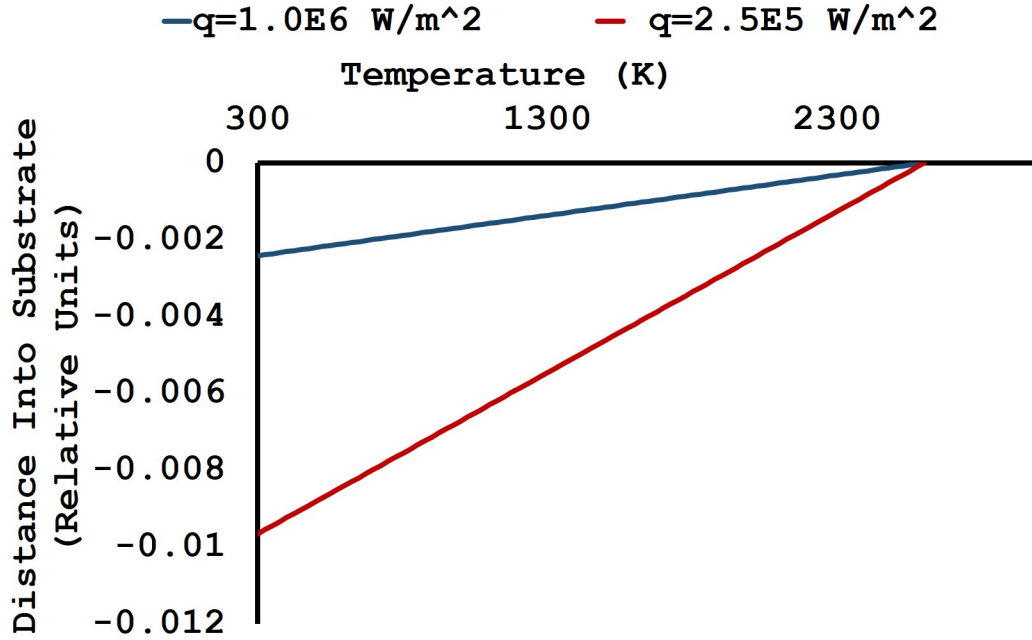


Fig. 3.12: Thermal profile into substrate.

equilibrium calculations modeling the constant volume combustion chamber. Combining the trends of burning time and heat release allows for the creation of ink formulations with the same amount of total energy release, but with differing rates of release.

The third criterion for successful bonding is a continuously interlaced bonding agent. Tin, the bonding agent used in the previously described experiments, fulfilled this criterion and provided a continuous structure on the macro-scale. We confirmed the presence of a continuous structure by measuring the electrical resistance across the entire length of the line. Despite a continuous path being present, we note that images show the line is still porous on the micron-scale (see Figure 3.14). The

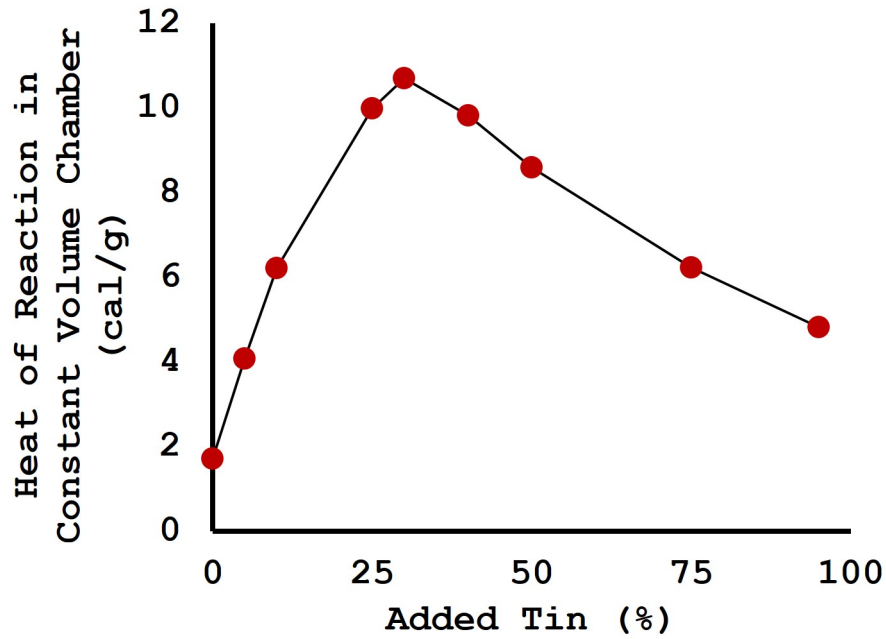
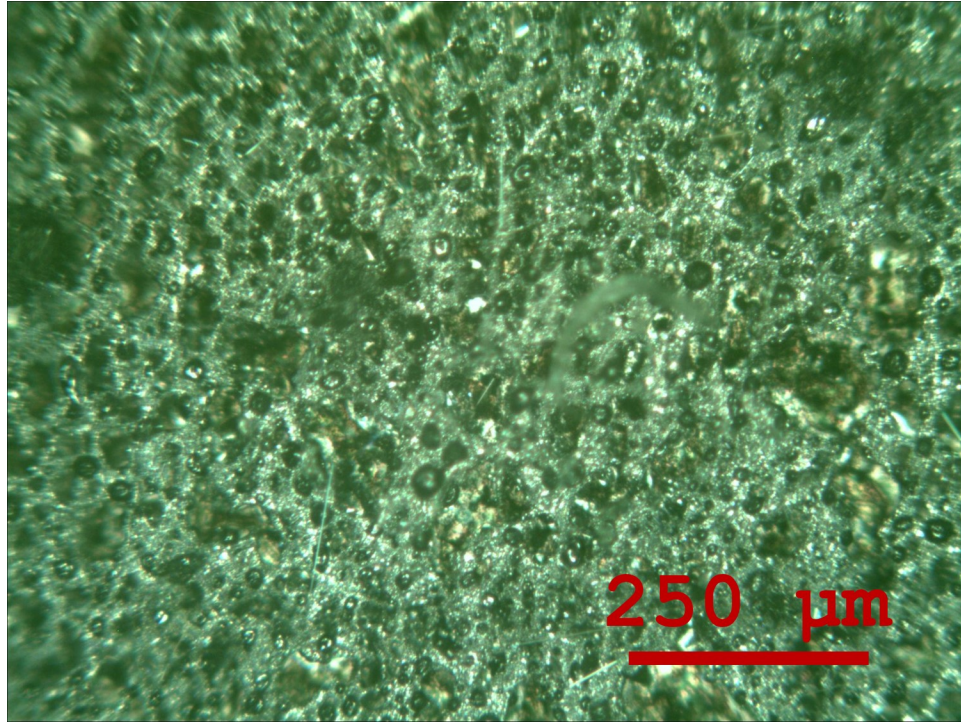


Fig. 3.13: Heat of reaction vs. added tin.

nanoscale tin particles agglomerate to form a bed of micron-scale particles sintered together.

As discussed in Section 1.3, a mechanism for binding the substrate to the bulk bonding material is required. In these experiments, we exploit the alloying reaction between elemental tungsten and elemental silicon. Elemental tungsten is produced after losing its oxygen to aluminum. Additionally, the aluminum scavenges oxygen from silicon dioxide present on the surface of the soda-lime glass substrate, yielding exposed elemental silicon. The feasibility of this reaction is tested with thermochemical equilibrium calculations by reacting a composition of 80 wt. percent stoichiometric aluminum tungsten trioxide and 20 wt. percent silicon dioxide.



*Fig. 3.14:* Continuous bonding material layer is porous on a micron-scale.

A significant portion of silicon dioxide is seen to reduce to elemental silicon while maintaining an adiabatic temperature around 2500 K. Therefore, we posit this alloying reaction is forming a bond between the bulk bonding material and the soda-lime glass substrate as seen in the phase diagram in Figure 3.15, reproduced from [6].

An SEM image of the cross section of a bonded slide provides more concrete evidence of the proposed adhesion mechanism. The EDS line scan in Figure 3.16 indicates tungsten silicon concentrations following a constant 6:4 ratio across the bonded region until the edge of the substrate, where the concentration of tungsten begins to decrease. This 6:4 ratio of tungsten to silicon corresponds with a eutectic point at

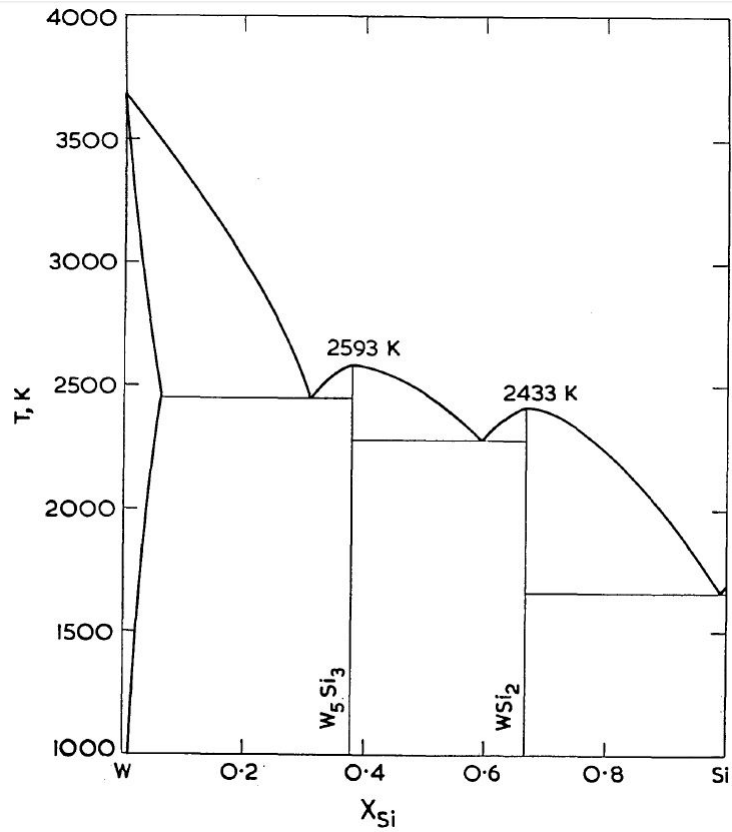


Fig. 3.15: Tungsten silicon system phase diagram [6].

2433 K. Spacial EDS mapping in Figure 3.17 shows micron-scale particles of tungsten and silicon that have formed away from the substrate surface. The approximate location of this micron-scale particle is outlined in blue in Figure 3.16. EDS mapping corresponds to elemental intensity but not necessarily to atomic percentages. We are unable to identify the specific alloy with certainty. However, the consistency of the ratio is indicative of a single alloy, rather than a mixture of alloys.

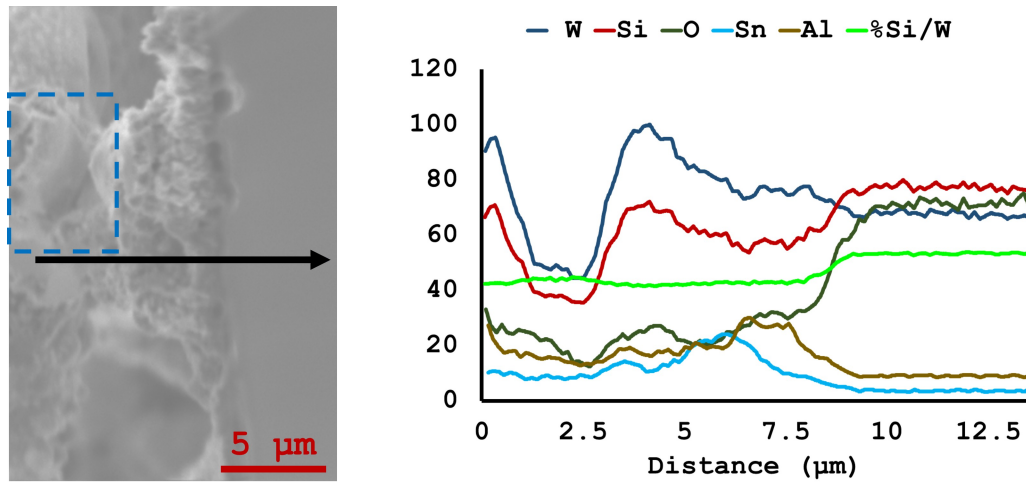


Fig. 3.16: EDS line scan of substrate surface bonding.

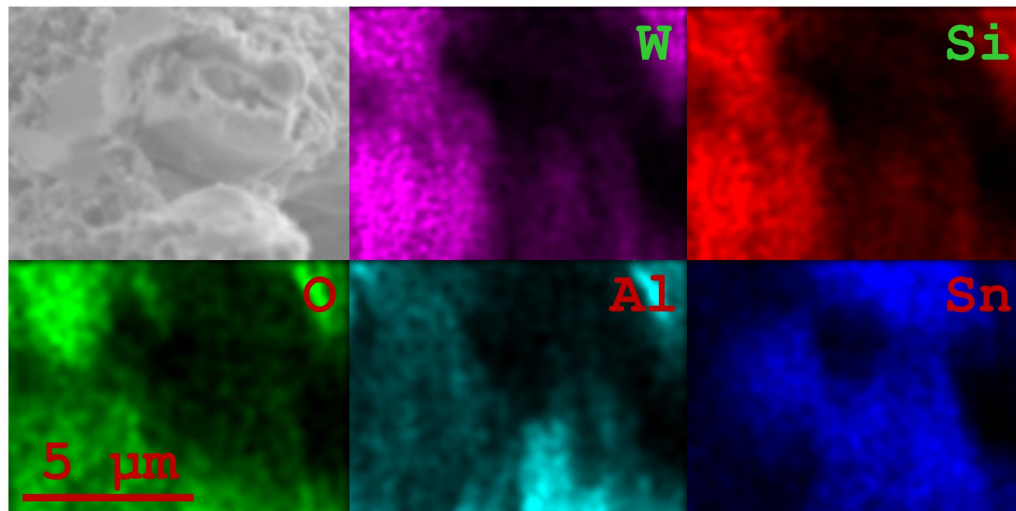


Fig. 3.17: EDS map showing tungsten silicon alloying away from substrate surface.

### 3.4 Stress Testing

Bonded slide pairs are observed to exhibit two possible failure mechanisms corresponding to the two regions of the bond. The first bond region is between the

bonding agent particles (e.g., between tin particles). The second region of the bond is between the bonding material and the substrate surface (e.g., between the Al/WO<sub>3</sub>/tin mixture and the soda-lime glass surface). The weaker of the two bonding regions will fail first during loading.

The first failure mechanism depends solely on the strength of the bonding agent and quality of the bond between bonding agent clusters. Figure 3.14 indicates the reaction reaches the melting temperature of the tin, which allows it to locally melt, flow freely, and coalesce. This creates a macro-scale bonded network of sintered micron particles. The bonds between these micron particles failed under loading. Improving the ability of local tin to flow and combine with tin in nearby regions increases the strength in this region of the bond. The easiest solution is to increase the percentage of added tin. This would decrease the distance liquid tin must flow to join a neighboring melted mass. However, increasing the percentage of added tin also increases the burning time and heat transfer to the substrate.

The second failure mechanism is dependent on the interface between the bulk bonding material and the substrate surface. During the previously described experiments, the bond created between the bulk bonding material and the substrate through the alloying of tungsten and silicon proved to be very strong. We were unable to load the sample until this bond failed due to other weaker links in the system. The bonding reaction proved to physically compromise the substrate surface by creating thermal fractures. The heat transfer to the substrate must be better controlled to

avoid this mechanism of failure in the future.

Experimental data, plotted in Figure 3.18, show the strongest bonds corresponds to 50% added tin with a bond thickness between 50-60  $\mu\text{m}$ . This thickness aligns closely with the minimum thickness of material required to propagate a reaction.

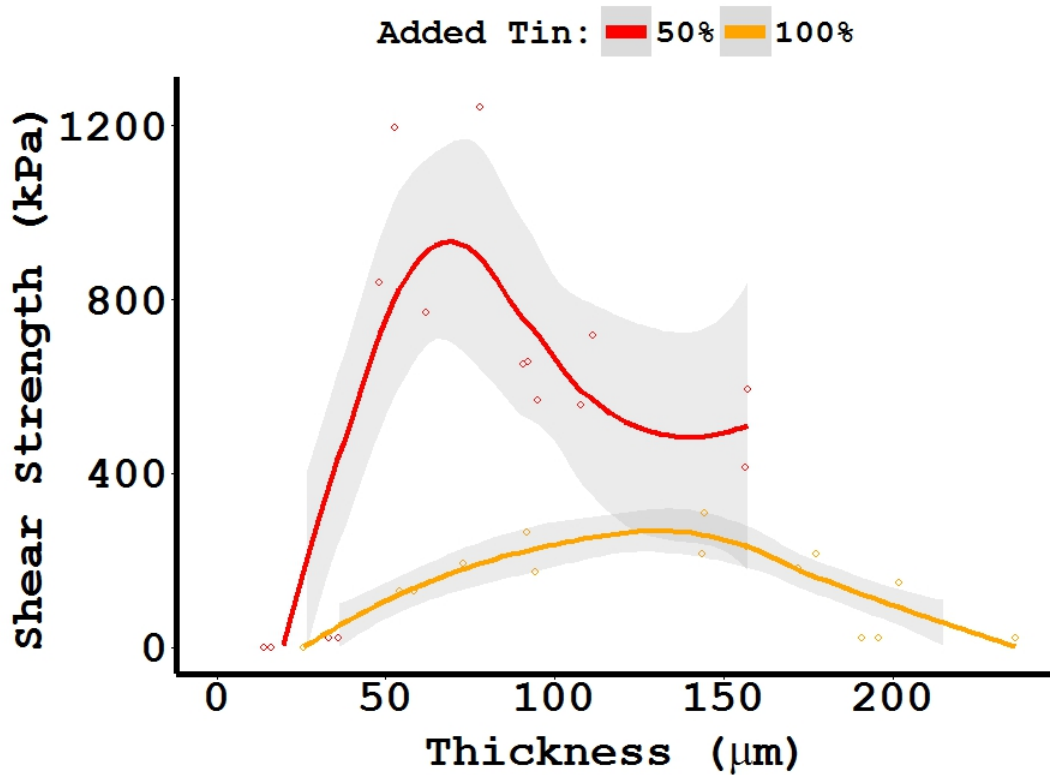


Fig. 3.18: Shear strength vs. thickness for 50% and 100% added nanotin.

The strongest bonded pairs failed in the bulk bonded material, i.e., bonds between tin particles pulled apart. Figure 3.19 shows a pair of substrates after a failure of the bulk bonded material. After failure, the tin remained continuous on the surface of

each substrate. An electrical resistance can be measured along the length of this line.



*Fig. 3.19:* The bonding material remains attached to both sides of the substrate during the first type of failure mechanism.

Higher percentages of tin and thicker bonding layers failed at the bond/substrate interface. In general, the soda-lime glass experienced varying degrees of thermal fracture as shown in the plan view Figure 3.20. Regions with thermal fractures proved to be very weak and failed under loading. During failure, the thermally-fractured regions would remain attached to the bulk bonded region but pull away from the substrate.

After failure, the substrate surface has regions of exposed bulk bonding material and exposed substrate. Figure 3.21 shows a plan view of the substrate surface after such a failure. A region of exposed thermally-fractured substrate is visible on the left and outlined in red. A second region still bonded to the now-fractured adjacent substrate is visible on the right outlined in blue. These two regions are separated by only 50 to a 100 microns of exposed bonding material.



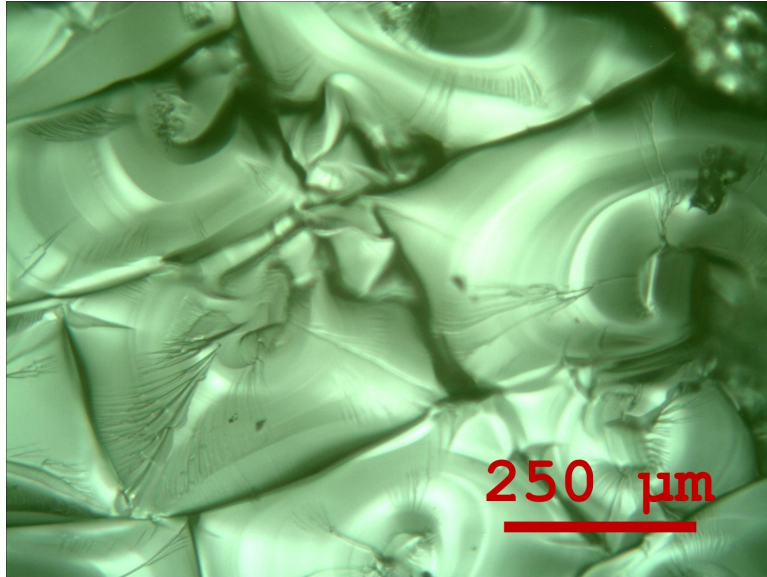


*Fig. 3.20:* Thermal fractures seen in substrates (1).

Interestingly, the bond between the substrate and bulk bonding material proved to be very strong and did not typically fail in either case. Figure 3.22 shows a fracture cross section view of a substrate with bulk bonding material and broken sections of the adjacent substrate remaining attached to the bulk material after failure.

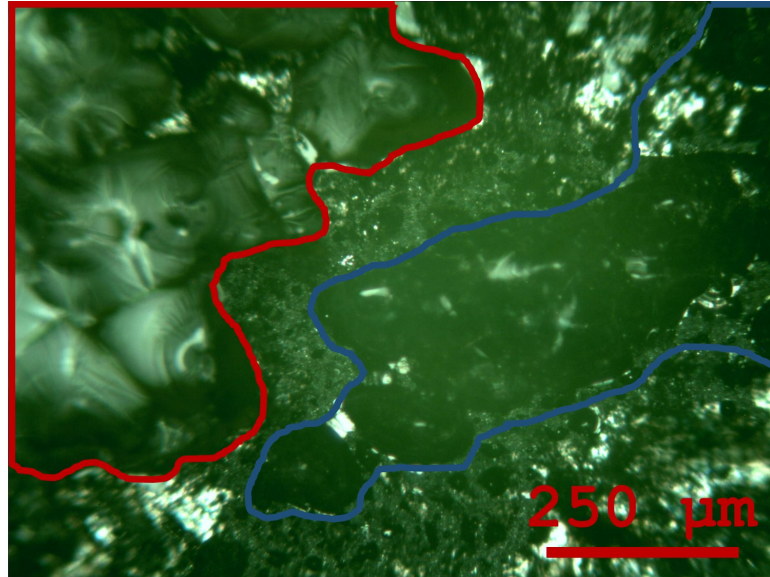


*Fig. 3.21:* Thermal fractures seen in substrates (2).

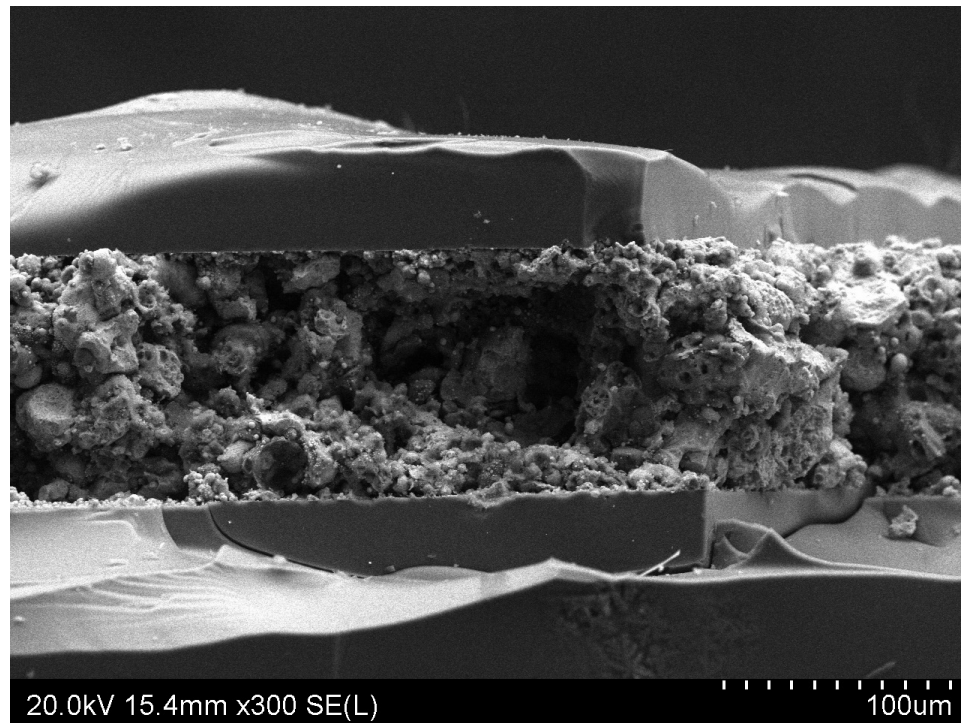


*Fig. 3.22:* Fragments of adjacent substrate remains bonded to bulk bonded region.

## Chapter 4: Conclusion

This work investigated the requirements to join nonmentals using aluminum-based nanoenergetics. Requirements for successful bonding were explored and four key criteria were established. First, a reactant system must not be chosen from the systems known to produce gas at the adiabatic flame temperature or in final products. Second, a reactant system must have tailored heat release rate and quantity to the specific substrates being bonded. Third, the product species must have a continuous bonding agent network throughout. Lastly, the system must have a mechanism to bond to the substrates being bonded. Based on these criteria, tungsten trioxide was selected as the oxidizer species due to the small amount of gaseous species generated during its combustion with aluminum. Tin was chosen as the bonding agent for its low melting temperature and low latent heat of fusion. The effect of a diluent on the nanothermite system was explored through simulation and thermochemical equilibrium calculations. The simulation indicated the number of interfaces between fuel and oxidizer particles decreases to only 25% of the ideal scenario and nearly half of its initial value for a sample with 100% added tin. It is clear a reaction that relies heavily on a large interface area will be negatively affected by the addition of large amounts of diluent. Furthermore, thermochemical equilibrium calculations

show small percentages of added tin promote gas generation and aid in reaction kinetics. However, higher percentages of tin will hinder the reaction, decreasing the adiabatic temperature until the reaction is eventually quenched. These theoretical results were compared with constant volume combustion experiments. Experimental results indicate a small or even negative effect on the reaction for percentages of tin less than 25%. An increase in gas generation and decrease in burning time is shown for added tin between 25% and 100%. Formulations with greater than 100% added tin experience substantially longer burning times and reduced reactivity. Measurements of combustion velocity indicated little change between lines open to the atmosphere and those confined with an adjacent substrate. Strength testing of bonded slides showed 50  $\mu\text{m}$  thick lines containing 50% added tin produced the strongest bonds. In several cases, these bonds failed above 1200 kPa. The bonds were seen to fail by two mechanisms. The first mechanism was within the bulk bonding material, and failure occurred between large tin clusters. A second possible failure mechanism was between the bulk bonding material and the substrate surface. Tungsten and silicon alloyed, producing a very strong bond which did not fail during our tests. However, the substrates often experienced thermal fractures which compromised the strength of the surface and lead to failure. This work acts as a framework which can be built upon to establish a library of “ink” formulations that can be used with a range of materials in a variety of applications. The ink formulation technique presented here has also been used to bond bulk copper to a soda-lime glass substrate. Although an in depth analysis of this application has yet to be completed, this method holds promise for providing an effective way to join

nonmetal surfaces.

## Bibliography

- [1] B. Bockmon, M. Pantoya, S. Son, B. Asay, and J. Mang. Combustion velocities and propagation mechanisms of metastable interstitial composites. *Journal of Applied Physics*, 98(6):064903–064903, 2005.
- [2] G. Bohlouli Zanjani. Synthesis, characterization, and application of nanothermites for joining. 2013.
- [3] M. P. Borom and J. A. Pask. Role of adherence oxides in the development of chemical bonding at glass-metal interfaces. *Journal of the American Ceramic Society*, 49(1):1–6, 1966.
- [4] J. J. Brennan and J. A. PASK. Effect of composition on glass-metal interface reactions and adherence. *Journal of the American Ceramic Society*, 56(2):58–62, 1973.
- [5] G. Caswell. Nanobond® assembly—a rapid, room temperature soldering process. In *Microelectronics and Packaging Conference, 2009. EMPC 2009. European*, pages 1–6. IEEE, 2009.
- [6] T. Chart. Thermodynamic properties of the tungsten–silicon and chromium–silicon systems. *Metal Science*, 9(1):504–509, 1975.

- [7] W. Danen and J. Martin. Energetic composites, Nov. 30 1993. US Patent 5,266,132.
- [8] M. Despont, H. Gross, F. Arrouy, C. Stebler, and U. Staufer. Fabrication of a silicon-pyrex-silicon stack by ac anodic bonding. *Sensors and Actuators A: Physical*, 55(2):219–224, 1996.
- [9] D. Dlott. Thinking big (and small) about energetic materials. *Materials science and technology*, 22(4):463–473, 2006.
- [10] I. Donald. Preparation, properties and chemistry of glass-and glass-ceramic-to-metal seals and coatings. *Journal of materials science*, 28(11):2841–2886, 1993.
- [11] E. L. Dreizin. Metal-based reactive nanomaterials. *Progress in Energy and Combustion Science*, 35(2):141–167, 2009.
- [12] H. Duan, C. Li, W. Yang, B. Lojewski, L. An, and W. Deng. Near-field electro spray microprinting of polymer-derived ceramics. *Microelectromechanical Systems, Journal of*, 22(1):1–3, 2013.
- [13] J. Eckert, J. Holzer, C. Ahn, Z. Fu, and W. Johnson. Melting behavior of nanocrystalline aluminum powders. *Nanostructured materials*, 2(4):407–413, 1993.
- [14] S. H. Fischer and M. Grubelich. Theoretical energy release of thermites, intermetallics, and combustible metals. Technical report, Sandia National Labs., Albuquerque, NM (US), 1998.

- [15] T. J. Foley, S. Son, V. E. Sanders, and B. Asay. The effect of added alumina on the propagation behavior of the nanoaluminum and molybdenum (vi) oxide system. In *Proceedings of the Thirteenth International Detonation Symposium, Norfolk, VA*, pages 23–28, 2006.
- [16] R. Givens, J. Klein, T. Burky, and J. Reuther. Thermite charge, July 7 2009. US Patent 7,555,986.
- [17] H. Goldschmidt. Method of producing metals and alloys., Mar. 16 1897. US Patent 578,868.
- [18] H. Goldschmidt. Process of metal-welding., Aug. 4 1903. US Patent 735,244.
- [19] U. Gösele, H. Stenzel, T. Martini, J. Steinkirchner, D. Conrad, and K. Scheerschmidt. Self-propagating room-temperature silicon wafer bonding in ultrahigh vacuum. *Applied physics letters*, 67(24):3614–3616, 1995.
- [20] C. H and H. B. Incendiary bomb mixture, July 20 1948. US Patent 2,445,312.
- [21] J. Healy and A. Andrews. The cobalt-reduction theory for the adherence of sheet-iron ground coats. *Journal of the American Ceramic Society*, 34(7):207–214, 1951.
- [22] M. L. Hobbs, M. R. Baer, and B. C. McGee. Jczs: An intermolecular potential database for performing accurate detonation and expansion calculations. *Propellants Explosives Pyrotechnics*, 24(5):269–279, 1999.



- [23] D. Housed. Welding of railroad rails a literature and industry survey'. *Rail Steels: Developments, processing, and use*, 644:118, 1978.
- [24] A. Il'in, A. Gromov, V. Vereshchagin, E. Popenko, V. Surgin, and H. Lehn. Combustion of ultrafine aluminum in air. *Combustion, Explosion and Shock Waves*, 37(6):664–668, 2001.
- [25] B. W. King, H. Tripp, and W. H. Duckworth. Nature of adherence of porcelain enamels to metals. *Journal of the American Ceramic Society*, 42(11):504–525, 1959.
- [26] Y.-S. Kwon, A. A. Gromov, A. P. Ilyin, E. M. Popenko, and G.-H. Rim. The mechanism of combustion of superfine aluminum powders. *Combustion and flame*, 133(4):385–391, 2003.
- [27] J. MCLAIN. Pyrotechnics: From the viewpoint of solid state chemistry(book). *Philadelphia, Pa., Franklin Institute Press, 1980. 252 p*, 1980.
- [28] E. B. Motlagh, J. V. Khaki, and M. H. Sabzevar. Welding of aluminum alloys through thermite like reactions in al-cuo-ni system. *Materials Chemistry and Physics*, 133(2):757–763, 2012.
- [29] R. G. Nuzzo, B. R. Zegarski, and L. H. Dubois. Fundamental studies of the chemisorption of organosulfur compounds on gold (111). implications for molecular self-assembly on gold surfaces. *Journal of the American Chemical Society*, 109(3):733–740, 1987.

- [30] M. L. Pantoya and J. J. Granier. Combustion behavior of highly energetic thermites: Nano versus micron composites. *Propellants, Explosives, Pyrotechnics*, 30(1):53–62, 2005.
- [31] J. A. Pask and R. M. Fulrath. Fundamentals of glass-to-metal bonding: Viii, nature of wetting and adherence. *Journal of the American Ceramic Society*, 45(12):592–596, 1962.
- [32] P. Peng, A. Hu, A. P. Gerlich, Y. Liu, and Y. N. Zhou. Self-generated local heating induced nanojoining for room temperature pressureless flexible electronic packaging. *Scientific reports*, 5, 2015.
- [33] A. Pivkina, P. Ulyanova, Y. Frolov, S. Zavyalov, and J. Schoonman. Nanomaterials for heterogeneous combustion. *Propellants, Explosives, Pyrotechnics*, 29(1):39–48, 2004.
- [34] P. Pranda, K. Prandova, and V. Hlavacek. Particle size and reactivity of aluminum powders. *Combustion science and technology*, 156(1):81–96, 2000.
- [35] V. Rozenband and N. Vaganova. A strength model of heterogeneous ignition of metal particles. *Combustion and Flame*, 88(1):113–118, 1992.
- [36] J. Shen, Z. Qiao, K. Zhang, J. Wang, R. Li, H. Xu, G. Yang, and F. Nie. Effects of nano-ag on the combustion process of al–cuo metastable intermolecular composite. *Applied Thermal Engineering*, 62(2):732–737, 2014.
- [37] M. Shimbo, K. Furukawa, K. Fukuda, and K. Tanzawa. Silicon-to-silicon direct bonding method. *Journal of Applied Physics*, 60(8):2987–2989, 1986.

- [38] E. Song. Thermite destructive device, Dec. 16 1997. US Patent 5,698,812.
- [39] H. F. STALEY. Electrolytic reactions in vitreous enamels and their relation to the adherence of enamels to steel\*. *Journal of the American Ceramic Society*, 17(1-12):163–167, 1934.
- [40] K. Sullivan. Ignition, combustion and tuning of nanocomposite thermites. *ProQuest Dissertations and Theses*, page 255, 2010.
- [41] A. Swiston, T. Hufnagel, and T. Weihs. Joining bulk metallic glass using reactive multilayer foils. *Scripta Materialia*, 48(12):1575–1580, 2003.
- [42] A. P. Tomsia and J. A. Pask. Bonding of dental glass to nickel-chromium alloys. *Journal of the American Ceramic Society*, 69(10):C–239, 1986.
- [43] M. A. Trunov, M. Schoenitz, X. Zhu, and E. L. Dreizin. Effect of polymorphic phase transformations in  $\text{Al}_2\text{O}_3$  film on oxidation kinetics of aluminum powders. *Combustion and Flame*, 140(4):310–318, 2005.
- [44] L. Wang, Z. Munir, and Y. M. Maximov. Thermite reactions: their utilization in the synthesis and processing of materials. *Journal of Materials Science*, 28(14):3693–3708, 1993.
- [45] R. Wolffenbuttel and K. Wise. Low-temperature silicon wafer-to-wafer bonding using gold at eutectic temperature. *Sensors and Actuators A: Physical*, 43(1):223–229, 1994.